Exclusive $f_1(1285)$ meson production for energy ranges available at the GSI-FAIR with HADES and PANDA

Piotr Lebiedowicz,[1,*] Otto Nachtmann,[2,†] Piotr Salabura,[3,‡] and Antoni Szczurek[1,§]

[1]*Institute of Nuclear Physics Polish Academy of Sciences, Radzikowskiego 152, PL-31342 Kraków, Poland*
[2]*Institut für Theoretische Physik, Universität Heidelberg, Philosophenweg 16, D-69120 Heidelberg, Germany*
[3]*M. Smoluchowski Institute of Physics, Jagiellonian University, Łojasiewicza 11, PL-30348 Kraków, Poland*

(Received 27 May 2021; accepted 16 July 2021; published 30 August 2021)

We evaluate the cross section for the $pp \to ppf_1(1285)$ and $p\bar{p} \to p\bar{p}f_1(1285)$ reactions at near threshold energies relevant for the HADES and PANDA experiments at GSI-FAIR. We assume that at energies close to the threshold the $\omega\omega \to f_1(1285)$ and $\rho^0\rho^0 \to f_1(1285)$ fusion processes are the dominant production mechanisms. The vertex for the $VV \to f_1$ coupling is derived from an effective coupling Lagrangian. The $g_{\rho\rho f_1}$ coupling constant is extracted from the decay rate of $f_1(1285) \to \rho^0\gamma$ using the vector-meson-dominance ansatz. We assume $g_{\omega\omega f_1} = g_{\rho\rho f_1}$, equality of these two coupling constants, based on arguments from the naive quark model and vector-meson dominance. The amplitude for the $VV \to f_1$ fusion, supplemented by phenomenological vertex form factors for the process, is given. The differential cross sections at energies close to the threshold are calculated. In order to determine the parameters of the model the $\gamma p \to f_1(1285)p$ reaction is discussed in addition and results are compared with the CLAS data. The possibility of a measurement by HADES@GSI is presented and discussed. We perform a Monte Carlo feasibility simulation of the $pp \to ppf_1$ reaction for $\sqrt{s} = 3.46$ GeV with the f_1 decaying into the $\pi^+\pi^-\pi^+\pi^-$ (not shown explicitly) and $\pi^+\pi^-\eta(\to \pi^+\pi^-\pi^0)$ final states using the PLUTO event generator. The latter f_1 decay is especially promising as a peak in the $\pi^+\pi^-\eta$ mass distribution should be observable by HADES.

DOI: 10.1103/PhysRevD.104.034031

I. INTRODUCTION

The production of light axial-vector mesons with quantum numbers $I^G J^{PC} = 0^+1^{++}$ is very interesting and was discussed in a number of experimental and theoretical papers. For example, the $f_1(1285)$ meson was measured in two-photon interactions in the reaction $e^+e^- \to e^+e^-\eta\pi^+\pi^-(\eta \to \gamma\gamma)$ by the Mark II [1], the TPC/Two-Gamma [2,3], and, more recently, by the L3 [4] collaborations. In such a process the $\gamma^*\gamma^* \to f_1(1285)$ vertex, associated with corresponding transition form factors, is the building block in calculating the amplitude. Different vector-vector-f_1 vertices and corresponding transition form factors were suggested in the literature [5–14]. It was suggested in [15] that a measurement of the $e^+e^- \to e^+e^-f_1(1285)$ reaction with double tagging at Belle II at KEK could shed new light on the $\gamma^*\gamma^*f_1$ coupling with two virtual photons.

The $f_1(1285)$ meson was also measured in the photoproduction process $\gamma p \to f_1(1285)p$ by the CLAS Collaboration at JLAB [16]. The differential cross sections were measured from threshold up to a center-of-mass energy of $W_{\gamma p} = 2.8$ GeV in a wide range of production angles. The $f_1(1285)$ photoproduction was studied extensively from the theoretical point of view; see [17–21]. There, the t-channel ρ and ω exchange (either Regge trajectories or meson exchanges) is the dominant reaction mechanism for the small-t behavior of the cross section, that is, in the forward scattering region. The contribution of the u-channel proton-exchange term with the coupling of $f_1(1285)$ to the nucleon is dominant at the backward angles [18–20,22]. In [20] the authors showed that also the s-channel nucleon resonance $N(2300)$ with $J^P = 1/2^+$ may play an important role in the reaction of $\gamma p \to f_1(1285)p$

*Piotr.Lebiedowicz@ifj.edu.pl
†O.Nachtmann@thphys.uni-heidelberg.de
‡Piotr.Salabura@uj.edu.pl
§Antoni.Szczurek@ifj.edu.pl
Also at College of Natural Sciences, Institute of Physics, University of Rzeszów, ul. Pigonia 1, PL-35310 Rzeszów, Poland.

around $\sqrt{s} = 2.3$ GeV. As was shown in [20] other contributions, the s-channel proton-exchange term, the u-channel $N(2300)$-exchange term, and the contact term, are very small and can be neglected in the analysis of the CLAS data. The Primakoff effect by the virtual photon exchange in the t-channel was discussed in [21]. This mechanism is especially important in the forward region and at higher $W_{\gamma p}$ energies.

The $pp \to ppf_1(1285)$ reaction was already measured by the WA102 Collaboration for center-of-mass energies $\sqrt{s} = 12.7$ and 29.1 GeV [23–26]. There the dominant contribution at $\sqrt{s} = 29.1$ GeV is most probably related to the double-Pomeron-exchange ($\mathbb{PP}$-fusion) mechanism; see [27]. In [27] the $pp \to ppf_1(1285)$ and $pp \to ppf_1(1420)$ reactions were considered in the tensor-Pomeron approach [28]. A good description of the WA102 data [25] at $\sqrt{s} = 29.1$ GeV was achieved. A study of central exclusive production (CEP) of the axial vector mesons f_1 at high energies (RHIC, LHC) could shed more light on the coupling of two Pomerons to the f_1 meson [27]. As discussed in Appendix D of [27] at the lower energy $\sqrt{s} = 12.7$ GeV the Reggeized-vector-meson-exchange or Reggeon-Reggeon-exchange contributions should be taken into account.

The $\omega\omega \to f_1$ and $\rho^0\rho^0 \to f_1$ fusion are the most probable low energy production processes. We know how the ω and ρ^0 couple to nucleons. However, the couplings of $\omega\omega \to f_1$ and $\rho^0\rho^0 \to f_1$ are less known. We note that future experiments at HADES and PANDA will provide new information there. The $\rho^0\rho^0 \to f_1(1285)$ coupling constant can be obtained from the decays: $f_1 \to \rho^0\gamma$ and/or $f_1 \to \pi^+\pi^-\pi^+\pi^-$.

In the present analysis we obtain the $g_{\rho\rho f_1}$ coupling constant from the radiative decay process $f_1(1285) \to \gamma\rho^0 \to \gamma\pi^+\pi^-$ using the vector-meson-dominance (VMD) ansatz; see Appendices A and B. We discuss briefly our results for the $\gamma p \to f_1(1285)p$ reaction and compare with the CLAS data in Appendix C. From this comparison we estimate the form-factor cutoff parameters.

The PANDA experiment (antiProton ANnihilations at DArmstadt) [29] will be one of the key experiments at the Facility for Antiproton and Ion Research (FAIR) which is currently being constructed. At FAIR, a system of accelerators and storage rings will be used to generate a beam of antiprotons with a momentum between 1.5 and 15 GeV/c. The design maximum energy in the center-of-mass (c.m.) system for antiproton-proton collisions is $\sqrt{s} \simeq 5.5$ GeV.

The exclusive production of the $f_0(1500)$ meson in antiproton-proton collisions via the pion-pion fusion mechanism was discussed for the PANDA experiment in [30]; see also Fig. 3 of [31]. The pion-pion fusion contribution grows quickly from the threshold, has a maximum at $\sqrt{s} \simeq 6$ GeV and then drops slowly with increasing energy. The predicted cross section for the $p\bar{p}f_0(1500)$ final state is $\sigma_{f_0} = 0.3$–0.8 μb for $\sqrt{s} = 5.5$ GeV; see Sec. III C of [30]. At intermediate energies (e.g., for the WA102 and COMPASS experiments) other exchange processes such as the Reggeon-Reggeon, Reggeon-Pomeron and Pomeron-Pomeron exchanges are very probable; see e.g., [31].

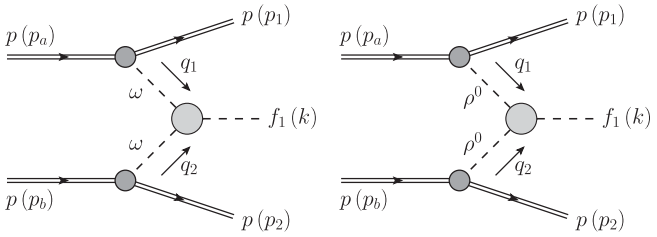

FIG. 1. The VV-fusion mechanisms (VV stands for $\omega\omega$ or $\rho^0\rho^0$) for f_1 production in proton-proton collisions.

A measurement at low energies, such as HADES@GSI would be interesting to impose constraints on the $VV \to f_1(1285)$ vertices. In this paper we wish to make first estimates of the total and differential cross sections for the $pp \to ppf_1(1285)$ and $p\bar{p} \to p\bar{p}f_1(1285)$ reactions at energies relevant for the HADES and PANDA experiments. We shall present some differential distributions for the HADES energy at $\sqrt{s} = 3.46$ GeV and for the future experiments with the PANDA detector at $\sqrt{s} = 5.0$ GeV. The experimental possibilities of such measurements will be discussed in addition.

II. THEORETICAL FRAMEWORK

A. $f_1(1285)$ meson production via $\omega\omega$ and $\rho\rho$ fusion mechanisms

We study central exclusive production of the $f_1(1285)$ in proton-proton collisions

$$p(p_a, \lambda_a) + p(p_b, \lambda_b) \to p(p_1, \lambda_1) + f_1(k, \lambda_{f_1}) + p(p_2, \lambda_2), \quad (2.1)$$

where $p_{a,b}$, $p_{1,2}$ and $\lambda_{a,b}$, $\lambda_{1,2} = \pm\frac{1}{2}$ denote the four-momenta and helicities of the protons, and k and $\lambda_{f_1} = 0, \pm 1$ denote the four-momentum and helicity of the f_1 meson, respectively.

In [27] for the reaction (2.1) the Pomeron-Pomeron-fusion mechanism was considered which seems to dominate at the WA102 energy of $\sqrt{s} = 29.1$ GeV. As discussed in Appendix D of [27] at lower energies other fusion mechanisms may be important. We shall take into account only the main processes at energies close to the threshold, the VV-fusion mechanism, shown by the diagrams in Fig. 1. There can also be the $a_0^0(980)\pi^0$- and $a_1^0(1260)\pi^0$-fusion mechanisms not considered in the present paper. Since the coupling constants $g_{a_0NN} \simeq 3.7$ [32–34] and $g_{f_1a_0\pi} = 2.5$ [35] are rather small we expect the $a_0^0(980)\pi^0$-fusion

mechanism to not give a sizeable contribution. Moreover, the form factors for virtual mesons at the a_0NN and $f_1a_0\pi$ vertices are rather poorly known. For the a_1 case, we expect that the $a_1(1260)$ meson propagator will reduce the cross section. Note that due to the large width of the $a_1(1260)$ the decay $f_1(1285) \to \pi^{\pm}a_1^{\mp}$ can easily occur for off-shell $a_1(1260)$ and this is an important decay mode in the $f_1 \to 2\pi^+2\pi^-$ channel as will be discussed in [36].

The kinematic variables for the reaction (2.1) are

$$\begin{aligned} &q_1 = p_a - p_1, \quad q_2 = p_b - p_2, \quad k = q_1 + q_2, \\ &t_1 = q_1^2, \quad t_2 = q_2^2, \quad m_{f_1}^2 = k^2, \\ &s = (p_a + p_b)^2 = (p_1 + p_2 + k)^2, \\ &s_1 = (p_a + q_2)^2 = (p_1 + k)^2, \\ &s_2 = (p_b + q_1)^2 = (p_2 + k)^2. \end{aligned} \tag{2.2}$$

For the kinematics see e.g., Appendix D of [31].

The amplitude for the reaction (2.1) includes two terms

$$\mathcal{M}_{pp\to ppf_1(1285)} = \mathcal{M}^{(\omega\omega\,\text{fusion})}_{pp\to ppf_1(1285)} + \mathcal{M}^{(\rho\rho\,\text{fusion})}_{pp\to ppf_1(1285)}. \tag{2.3}$$

The VV-fusion ($VV = \rho^0\rho^0$ or $\omega\omega$) amplitude can be written as

$$\begin{aligned} &\mathcal{M}^{(VV\,\text{fusion})}_{\lambda_a\lambda_b\to\lambda_1\lambda_2\lambda_{f_1}} \\ &\quad = (-i)(\epsilon^{\alpha}(\lambda_{f_1}))^*\bar{u}(p_1,\lambda_1)i\Gamma^{(Vpp)}_{\mu_1}(p_1,p_a)u(p_a,\lambda_a) \\ &\qquad \times i\tilde{\Delta}^{(V)\mu_1\nu_1}(s_1,t_1)i\Gamma^{(VVf_1)}_{\nu_1\nu_2\alpha}(q_1,q_2)i\tilde{\Delta}^{(V)\nu_2\mu_2}(s_2,t_2) \\ &\qquad \times \bar{u}(p_2,\lambda_2)i\Gamma^{(Vpp)}_{\mu_2}(p_2,p_b)u(p_b,\lambda_b). \end{aligned} \tag{2.4}$$

Here $\epsilon_\alpha(\lambda)$ is the polarization vector of the f_1 meson, $\Gamma^{(Vpp)}_{\mu}$ and $\Gamma^{(VVf_1)}_{\nu_1\nu_2\alpha}$ are the Vpp and VVf_1 vertex functions, respectively, and $\tilde{\Delta}^{(V)\mu\nu}$ is the propagator for the Reggeized vector meson V. At very low energies the latter must be replaced by $\Delta^{(V)\mu\nu}$, the standard propagator for the vector meson V. We shall now discuss all these quantities in turn.

First we discuss the VVf_1 coupling. We start by considering the on shell process of two real vector particles V fusing to give an f_1 meson:

$$V + V \to f_1. \tag{2.5}$$

The angular momentum analysis of such reactions was made in [31]. The spins of the two vectors can be combined to a total spin $S = 0, 1, 2$. Then S has to be combined with the orbital angular momentum l to give the spin $J = 1$ and parity $+1$ of the f_1 state. From Table VIII of [31] we find that there is here only one possible coupling, namely $(l, S) = (2, 2)$. A convenient corresponding coupling Lagrangian, given in (D9) of [27], reads

$$\begin{aligned} \mathcal{L}'_{VVf_1}(x) = &\frac{1}{M_0^4} g_{VVf_1}(V_{\kappa\lambda}(x)\overleftrightarrow{\partial}_\mu\overleftrightarrow{\partial}_\nu V_{\rho\sigma}(x)) \\ &\times (\partial_\alpha U_\beta(x) - \partial_\beta U_\alpha(x))g^{\kappa\rho}g^{\mu\sigma}\epsilon^{\lambda\nu\alpha\beta}, \end{aligned} \tag{2.6}$$

where

$$V_{\kappa\lambda}(x) = \partial_\kappa V_\lambda(x) - \partial_\lambda V_\kappa(x), \tag{2.7}$$

with $M_0 \equiv 1$ GeV and g_{VVf_1} a dimensionless coupling constant. $U_\alpha(x)$ and $V_\kappa(x)$ are the fields of the f_1 meson and the vector meson V, respectively. For the Levi-Civita symbol we use the normalization $\varepsilon_{0123} = +1$.

The expression for the VVf_1 vertex obtained from (2.6) is as follows

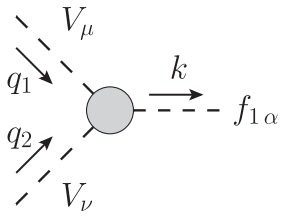

$$\begin{aligned} &i\Gamma^{(VVf_1)}_{\mu\nu\alpha}(q_1,q_2)|_{\text{bare}} \\ &= \frac{2g_{VVf_1}}{M_0^4}[(q_1-q_2)^\rho(q_1-q_2)^\sigma\varepsilon_{\lambda\sigma\alpha\beta}k^\beta \\ &\quad \times (q_{1\kappa}\delta^\lambda_\mu - q_1^\lambda g_{\kappa\mu})(q_2^\kappa g_{\rho\nu} - q_{2\rho}\delta^\kappa_\nu) + (q_1 \leftrightarrow q_2, \mu \leftrightarrow \nu)]; \end{aligned} \tag{2.8}$$

see (D11) of [27]. Here the label "bare" is used for a vertex as derived from (2.6) without a form-factor function. The vertex function (2.8) satisfies the relations

$$\begin{aligned} \Gamma^{(VVf_1)}_{\mu\nu\alpha}(q_1,q_2) &= \Gamma^{(VVf_1)}_{\nu\mu\alpha}(q_2,q_1), \\ \Gamma^{(VVf_1)}_{\mu\nu\alpha}(q_1,q_2)q_1^\mu &= 0, \\ \Gamma^{(VVf_1)}_{\mu\nu\alpha}(q_1,q_2)q_2^\nu &= 0, \\ \Gamma^{(VVf_1)}_{\mu\nu\alpha}(q_1,q_2)(q_1+q_2)^\alpha &= 0. \end{aligned} \tag{2.9}$$

For realistic applications we should multiply the 'bare' vertex (2.8) by a phenomenological cutoff function (form factor) F_{VVf_1} which we take in the factorized ansatz

$$F_{VVf_1}(q_1^2,q_2^2,k^2) = \tilde{F}_V(q_1^2)\tilde{F}_V(q_2^2)F_{f_1}(k^2). \tag{2.10}$$

We make the assumption that $\tilde{F}_V(t)$ is parametrized as

$$\tilde{F}_V(q^2) = \frac{\Lambda_V^4}{\Lambda_V^4 + (q^2 - m_V^2)^2}, \tag{2.11}$$

where the cutoff parameter Λ_V, taken to be the same for both ρ^0 and ω, is a free parameter. For the on-shell V and f_1 mesons we have $F_{VVf_1}(m_V^2, m_V^2, m_{f_1}^2) = 1$.

The vector-meson-(anti)proton vertex is [37]

$$i\Gamma_\mu^{(Vpp)}(p', p) = -i\Gamma_\mu^{(V\bar{p}\,\bar{p})}(p', p) = -ig_{Vpp}F_{VNN}(t)\left[\gamma_\mu - i\frac{\kappa_V}{2m_p}\sigma_{\mu\nu}(p - p')^\nu\right] \tag{2.12}$$

with the tensor-to-vector coupling ratio, $\kappa_V = f_{VNN}/g_{VNN}$. We use the following values for these coupling constants:

$$g_{\rho pp} = 3.0, \quad \kappa_\rho = 6.1, \quad g_{\omega pp} = 9.0, \quad \kappa_\omega = 0. \tag{2.13}$$

We give a short discussion of values for the ρpp and ωpp coupling constants found in the literature. For the ρNN coupling constants one finds $g_{\rho pp} = 2.63$–3.36 [38,39] and κ_ρ is expected to be $\kappa_\rho = 6.1 \pm 0.2$ [40]. There is a considerable uncertainty in the ωNN coupling constants. From Table I of [37] we see a broad range of values: $g_{\omega pp} \simeq 10$ to 21 and $\kappa_\omega \simeq -0.16$ to $+0.14$. For example, in [40] it was estimated $g_{\omega pp} = 20.86 \pm 0.25$ and $\kappa_\omega = -0.16 \pm 0.01$; see Table III of [40]. Within the (full) Bonn potential [32] values of $g_{\omega pp} = 15.85$ and $\kappa_\omega = 0$ are required for a best fit to NN scattering data. In [41] it was shown that such a fairly large value of $g_{\omega pp}$ must be considered as an effective coupling strength rather than as the intrinsic ωNN coupling constant. They found that the additional repulsion provided by the correlated $\pi\rho$ exchange to the NN interaction allows $g_{\omega NN}$ to be reduced by about a factor 2, leading to an "intrinsic" ωNN coupling constant which is more in line with the value one would obtain from the SU(3) flavor symmetry considerations, $g_{\omega NN} = 3g_{\rho NN}\cos(\Delta\theta_V)$ [39], where $\Delta\theta_V \simeq 3.7°$ is the deviation from the ideal $\omega - \phi$ mixing angle. The values of $g_{\omega pp} = 7.0$–10.5 and $\kappa_\omega \simeq 0$ were found to describe consistently the πN scattering and π photoproduction processes [42]. The values of $g_{\omega pp} = 9.0$ and $\kappa_\omega = -0.5$ have been used in the analysis of the $pp \to pp\omega$ reaction to reproduce the shape of the measured ω angular distribution; see Fig. 7 of [43]. It was shown [44] that the energy dependence of the total cross section and the angular distribution for $pp \to pp\omega$ can be described rather reasonably even with a vanishing κ_ω ($g_{\omega pp} = 9.0$, $\kappa_\omega = 0$); see Fig. 4 of [44]. Finally we note that in [28] the couplings of the $\omega_{\mathbb{R}}$ and $\rho_{\mathbb{R}}$ Reggeons to the proton were estimated from high-energy scattering data and found as

$$g_{\rho_{\mathbb{R}}pp} = 2.02 \quad \text{and} \quad g_{\omega_{\mathbb{R}}pp} = 8.65; \tag{2.14}$$

see (3.60) and (3.62) of [28]. Taking all this into account we think that our choice (2.13) for the coupling constants is quite reasonable.

The form factor $F_{VNN}(t)$ in (2.12), describing the t-dependence of the V-(anti)proton coupling, can be parametrized as

$$F_{VNN}(t) = \frac{\Lambda_{VNN}^2 - m_V^2}{\Lambda_{VNN}^2 - t}, \tag{2.15}$$

where $\Lambda_{VNN} > m_V$ and $t < 0$. Please note that the form factor $F_{VNN}(t)$ is normalized to unity at $t = m_V^2$. On the other hand, the Reggeon-proton couplings (2.14) are defined for $t = 0$. Since $F_{VNN}(0) < 1$ we expect that $g_{\rho_{\mathbb{R}}pp} < g_{\rho pp}$ and $g_{\omega_{\mathbb{R}}pp} < g_{\omega pp}$, which is indeed the case; see (2.13) and (2.14).

The coupling constant g_{VVf_1} and cutoff parameters Λ_V and Λ_{VNN} should be adjusted to experimental data. Examples are discussed in Appendices B and C. There, the form factor F_{VVf_1} (2.10) is used for $F_{f_1}(m_{f_1}^2) = 1$ and for different kinematic conditions of $\tilde{F}_V(q^2)$ (2.11), that is, for spacelike ($q^2 < 0$) and timelike ($q^2 > 0$) momentum transfers of the V meson, and also at $q^2 = 0$. In Appendix B we discuss the radiative decays of the $f_1(1285)$ meson in two ways $f_1 \to \rho\gamma$ (B1) and $f_1 \to (\rho^0 \to \pi^+\pi^-)\gamma$ (B2) where we have $F_{\rho\rho f_1}(m_\rho^2, 0, m_{f_1}^2)$ and $F_{\rho\rho f_1}(q^2 > 0, 0, m_{f_1}^2)$, respectively. In Table III in Appendix B we collect our results for $g_{\rho\rho f_1}$ extracted from the decay rate of $f_1 \to \rho^0\gamma$ using the VMD ansatz. The process $f_1 \to \rho^0\rho^0 \to 2\pi^+2\pi^-$, where both ρ^0 mesons carry timelike momentum transfers, will be studied in detail in [36]. For the $\gamma p \to f_1 p$ reaction, discussed in Appendix C, we have $F_{\rho\rho f_1}(0, q^2 < 0, m_{f_1}^2)$. This is closer to the $VV \to f_1$ fusion mechanisms shown in Fig. 1 where both V mesons have spacelike momentum transfers. From comparison of the model to the f_1-meson angular distributions of the CLAS experimental data [16] we shall extract the cutoff parameter Λ_{VNN} in the V-proton vertex (2.15); see (C7)–(C12) and Fig. 14 in Appendix C.

In the following we shall use the VVf_1 coupling (2.6) and the corresponding vertex (2.8)–(2.11) for our $VV \to f_1$ fusion processes of Fig. 1 for both: normal off-shell vector mesons V and Reggeized vector mesons V_R.

The standard form of the vector-meson propagator is given e.g., in (3.2) of [28]

$$i\Delta_{\mu\nu}^{(V)}(k) = i\left(-g_{\mu\nu} + \frac{k_\mu k_\nu}{k^2 + i\epsilon}\right)\Delta_T^{(V)}(k^2) - i\frac{k_\mu k_\nu}{k^2 + i\epsilon}\Delta_L^{(V)}(k^2). \tag{2.16}$$

With the relations from (2.9) for the VVf_1 vertex (2.8) the $k_\mu k_\nu$ term does not contribute in (2.4). For small values of $s_{1,2}$ and $|t_{1,2}|$ [see (2.2)] the simplest form of the transverse function, $\Delta_T^{(V)}(t) = (t - m_V^2)^{-1}$, should be adequate. For

higher values of s_1 and s_2 we must take into account Reggeization. We do this, following (3.21), (3.24) of [45], by making in (2.16) the replacements

$$\Delta_T^{(V)}(t_i) \to \tilde{\Delta}_T^{(V)}(s_i,t_i) = \Delta_T^{(V)}(t_i)\left(\exp(i\phi(s_i))\frac{s_i}{s_{\rm thr}}\right)^{\alpha_V(t_i)-1}, \tag{2.17}$$

where

$$\phi(s_i) = \frac{\pi}{2}\exp\left(\frac{s_{\rm thr}-s_i}{s_{\rm thr}}\right) - \frac{\pi}{2}, \tag{2.18}$$

for $i = 1$ or 2, and $s_{\rm thr}$ is the lowest value of s_i possible here:

$$s_{\rm thr} = (m_p + m_{f_1})^2. \tag{2.19}$$

We use the standard linear form for the vector meson Regge trajectories (cf., e.g., [46])

$$\alpha_V(t) = \alpha_V(0) + \alpha_V' t, \tag{2.20}$$

$$\alpha_V(0) = 0.5, \qquad \alpha_V' = 0.9\ \text{GeV}^{-2}. \tag{2.21}$$

Our Reggeized vector meson propagator, denoted by $\tilde{\Delta}_{\mu\nu}^{(V)}(s,t)$ is obtained from (2.16) with the replacement $\Delta_T^{(V)} \to \tilde{\Delta}_T^{(V)}$ from (2.17).

In the following we shall also consider the CEP of the $f_1(1285)$ with subsequent decay into $\rho^0\gamma$:

$$p(p_a,\lambda_a) + p(p_b,\lambda_b) \to p(p_1,\lambda_1) + [f_1(p_{34}) \to \rho^0(p_3,\lambda_3) + \gamma(p_4,\lambda_4)] + p(p_2,\lambda_2) \tag{2.22}$$

with $p_{34} = p_3 + p_4$. Here p_3, p_4 and $\lambda_3 = 0, \pm 1$, $\lambda_4 = \pm 1$ denote the four-momenta and helicities of the ρ^0 meson and the photon, respectively.

The amplitude for the reaction (2.22) can be written as in (2.4) but with the replacements

$$\begin{aligned} s_1 &\to \tilde{s}_1 = (p_1 + p_{34})^2, \\ s_2 &\to \tilde{s}_2 = (p_2 + p_{34})^2, \\ (\epsilon_\alpha^{(f_1)}(\lambda_{f_1}))^* &\to \frac{e}{\gamma_\rho}\Delta_T^{(f_1)}(p_{34}^2)\Gamma_{\rho\sigma\alpha}^{(\rho\rho f_1)}(-p_3,-p_4) \\ &\quad \times (\epsilon^{(\rho)\rho}(\lambda_3))^*(\epsilon^{(\gamma)\sigma}(\lambda_4))^*. \end{aligned} \tag{2.23}$$

Here $\epsilon^{(\rho)}$ and $\epsilon^{(\gamma)}$ are the polarization vectors of ρ^0 and γ, respectively, and $\Delta_T^{(f_1)}$ is the transverse part of the f_1 propagator which has a structure analogous to (2.16). The factor e/γ_ρ comes from the $\rho - \gamma$ transition vertex; see (3.23)–(3.25) of [28].

In practical calculations we introduce in the $\rho\rho f_1$ vertex the form factor $F_{f_1}(p_{34}^2)$ [see (2.10)] for the virtual f_1 meson

$$F_{f_1}(p_{34}^2) = \exp\left(\frac{-(p_{34}^2 - m_{f_1}^2)^2}{\Lambda_{f_1}^4}\right), \quad \Lambda_{f_1} = 1\ \text{GeV}. \tag{2.24}$$

In (2.23) we shall use a simple Breit-Wigner ansatz for the f_1 meson propagator

$$\Delta_T^{(f_1)}(p_{34}^2) = \frac{1}{p_{34}^2 - m_{f_1}^2 + i m_{f_1}\Gamma_{f_1}}. \tag{2.25}$$

The mass and total width of f_1 meson from [47] are

$$m_{f_1} = (1281.9 \pm 0.5)\ \text{MeV}, \tag{2.26}$$

$$\Gamma_{f_1} = (22.7 \pm 1.1)\ \text{MeV}. \tag{2.27}$$

We note that the mass of 1281.0 ± 0.8 MeV measured in the CLAS experiment [16] is in very good agreement with the PDG average value (2.26). The total width measured by the CLAS Collaboration is however smaller than the value (2.27):

$$\Gamma_{f_1} = (18.4 \pm 1.4)\ \text{MeV}. \tag{2.28}$$

For the proton-antiproton collisions we can write

$$\mathcal{M}_{p\bar{p}\to p\bar{p}f_1(1285)} = \mathcal{M}_{p\bar{p}\to p\bar{p}f_1(1285)}^{(\omega\omega\ \text{fusion})} + \mathcal{M}_{p\bar{p}\to p\bar{p}f_1(1285)}^{(\rho\rho\ \text{fusion})}. \tag{2.29}$$

Then the corresponding amplitudes are as in (2.4) but with the replacement

$$\begin{aligned} &\bar{u}(p_2,\lambda_2) i\Gamma_{\mu_2}^{(Vpp)}(p_2,p_b)u(p_b,\lambda_b) \\ &\quad \to \bar{v}(p_b,\lambda_b) i\Gamma_{\mu_2}^{(V\bar{p}\,\bar{p})}(p_2,p_b)v(p_2,\lambda_2) \\ &\quad = -\bar{u}(p_2,\lambda_2) i\Gamma_{\mu_2}^{(Vpp)}(p_2,p_b)u(p_b,\lambda_b). \end{aligned} \tag{2.30}$$

Using the V-(anti)proton coupling (2.12) in the VV-fusion amplitudes we obtain

$$\mathcal{M}_{p\bar{p}\to p\bar{p}f_1(1285)}^{(VV\ \text{fusion})} = -\mathcal{M}_{pp\to ppf_1(1285)}^{(VV\ \text{fusion})}. \tag{2.31}$$

B. Background processes to the $\rho\rho$ and $\rho\gamma$ channels of the f_1 decay in CEP

The main decay modes of the $f_1(1285)$ are [47] 4π, $\eta\pi\pi$, $K\bar{K}\pi$, and $\rho^0\gamma$. If the f_1 is to be identified and measured in CEP in any one of these channels one will have to consider background processes giving the same final state, for instance, $pp4\pi$. Therefore, in this section we discuss two background reactions: CEP of 4π via $\rho^0\rho^0$ in the continuum and CEP of $\rho^0\gamma$ in the continuum.

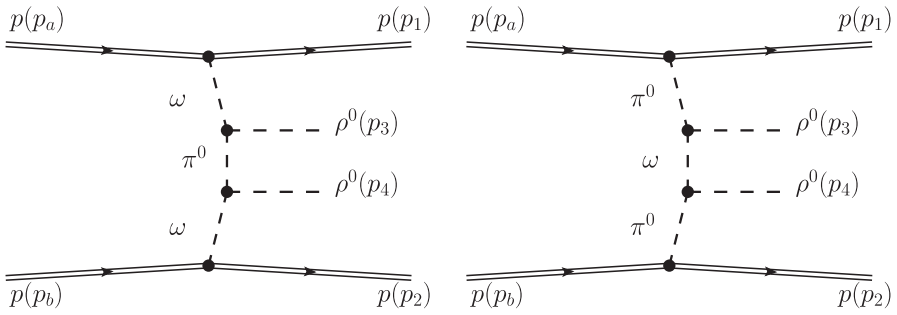

FIG. 2. Diagrams for exclusive continuum $\rho^0\rho^0$ production in proton-proton collisions. There are also the diagrams with $p_3 \leftrightarrow p_4$.

First we discuss the exclusive production of $\rho^0\rho^0$ in proton-proton collisions,

$$p(p_a,\lambda_a)+p(p_b,\lambda_b) \to p(p_1,\lambda_1)+\rho^0(p_3,\lambda_3)+\rho^0(p_4,\lambda_4)+p(p_2,\lambda_2), \quad (2.32)$$

where $p_{3,4}$ and $\lambda_{3,4}=0,\pm1$ denote the four-momenta and helicities of the ρ^0 mesons, respectively. In Fig. 2 we show the diagrams for two mechanisms which will contribute to the reaction (2.32) at low energies, $\omega\omega$ and $\pi^0\pi^0$ fusion.

There can also be the $\rho\rho$ fusion with exchange of an intermediate $\sigma \equiv f_0(500)$ meson and the $\sigma\sigma$ fusion with ρ^0 exchange. From the Bonn potential [32,48] we get for the squared coupling constant $g^2_{\sigma pp}/4\pi \simeq 6.0$ which is smaller than $g^2_{\pi pp}/4\pi \simeq 14.0$. Moreover, we can expect that $|g_{\sigma\rho\rho}| \ll |g_{\rho\omega\pi}|$. Due to large form-factor uncertainties and the poorly known $\sigma\rho\rho$ coupling we neglect these contributions in our present study. Other contributions may be due to the exchanges of the $f_2(1270)$ meson (f_2-ρ^0-f_2 or ρ^0-f_2-ρ^0) and the neutral $a_2(1320)$ meson (a_2-ω-a_2 or ω-a_2-ω). For the $f_2\rho\rho$ and $a_2\omega\rho$ couplings one could use the rather well-known couplings from (3.55), (3.56), (7.29)–(7.34) and (3.57), (3.58), (7.38)–(7.43) of [28], respectively. Since the f_2pp coupling, taking it equal to $f_{2\mathbb{R}}pp$ from (3.49), (3.50) of [28], is rather large, the f_2-ρ^0-f_2 fusion may give a large background contribution. Since $g_{\omega_{\mathbb{R}}pp} > g_{a_{2\mathbb{R}}pp}$, see (3.52) and (3.60) of [28], and the $a_2\omega\rho$ couplings have values similar to the $f_2\rho\rho$ couplings the $\omega - a_2 - \omega$ contribution may also be potentially important. However, we expect that the tensor meson propagator(s) will reduce the cross section for these processes.

At higher energies the Pomeron plus f_2 Reggeon ($\mathbb{P}+f_{2\mathbb{R}}$) fusion [($\mathbb{P}+f_{2\mathbb{R}}$)-$\rho^0$-($\mathbb{P}+f_{2\mathbb{R}}$)] and ρ^0 fusion with $\mathbb{P}+f_{2\mathbb{R}}$ exchange [ρ^0-($\mathbb{P}+f_{2\mathbb{R}}$)-$\rho^0$] will be important, probably the dominant processes; see [49]. We expect that these processes will give only a small contribution in the threshold region, of interest for us here. Therefore, we shall neglect also these mechanisms in the following.

With the assumption, motivated above, that the diagrams of Fig. 2 represent the dominant reaction mechanisms in the threshold region, the continuum amplitude for the reaction (2.32) can be written as

$$\mathcal{M}^{(\rho\rho\,\text{continuum})}_{pp\to pp\rho^0\rho^0} = \mathcal{M}^{(\omega\omega\,\text{fusion})}_{pp\to pp\rho^0\rho^0} + \mathcal{M}^{(\pi\pi\,\text{fusion})}_{pp\to pp\rho^0\rho^0}. \quad (2.33)$$

The $\omega\omega$- and $\pi\pi$-fusion amplitudes (2.33) are given by

$$\begin{aligned}\mathcal{M}^{(\omega\omega\,\text{fusion})}_{\lambda_a\lambda_b\to\lambda_1\lambda_2\lambda_3\lambda_4} &= (-i)(\epsilon^{(\rho)\rho_3}(\lambda_3))^*(\epsilon^{(\rho)\rho_4}(\lambda_4))^*\bar{u}(p_1,\lambda_1)i\Gamma^{(\omega pp)}_{\mu_1}(p_1,p_a)u(p_a,\lambda_a)\\ &\times[i\tilde{\Delta}^{(\omega)\mu_1\nu_1}(s_{13},t_1)i\Gamma^{(\rho\omega\pi)}_{\rho_3\nu_1}(p_3,q_1)i\Delta^{(\pi)}(p_t)i\Gamma^{(\rho\omega\pi)}_{\rho_4\nu_2}(p_4,q_2)i\tilde{\Delta}^{(\omega)\nu_2\mu_2}(s_{24},t_2)\\ &+i\tilde{\Delta}^{(\omega)\mu_1\nu_1}(s_{14},t_1)i\Gamma^{(\rho\omega\pi)}_{\rho_4\nu_1}(p_4,q_1)i\Delta^{(\pi)}(p_u)i\Gamma^{(\rho\omega\pi)}_{\rho_3\nu_2}(p_3,q_2)i\tilde{\Delta}^{(\omega)\nu_2\mu_2}(s_{23},t_2)]\\ &\times\bar{u}(p_2,\lambda_2)i\Gamma^{(\omega pp)}_{\mu_2}(p_2,p_b)u(p_b,\lambda_b),\end{aligned} \quad (2.34)$$

$$\begin{aligned}\mathcal{M}^{(\pi\pi\,\text{fusion})}_{\lambda_a\lambda_b\to\lambda_1\lambda_2\lambda_3\lambda_4} &= (-i)(\epsilon^{(\rho)\rho_3}(\lambda_3))^*(\epsilon^{(\rho)\rho_4}(\lambda_4))^*\bar{u}(p_1,\lambda_1)i\Gamma^{(\pi pp)}(p_1,p_a)u(p_a,\lambda_a)\\ &\times[i\Delta^{(\pi)}(q_1)i\Gamma^{(\rho\omega\pi)}_{\rho_3\nu_1}(p_3,-p_t)i\tilde{\Delta}^{(\omega)\nu_1\nu_2}(s_{34},p_t^2)i\Gamma^{(\rho\omega\pi)}_{\rho_4\nu_2}(p_4,p_t)i\Delta^{(\pi)}(q_2)\\ &+i\Delta^{(\pi)}(q_1)i\Gamma^{(\rho\omega\pi)}_{\rho_4\nu_1}(p_4,p_u)i\tilde{\Delta}^{(\omega)\nu_1\nu_2}(s_{34},p_u^2)i\Gamma^{(\rho\omega\pi)}_{\rho_3\nu_2}(p_3,-p_u)i\Delta^{(\pi)}(q_2)]\\ &\times\bar{u}(p_2,\lambda_2)i\Gamma^{(\pi pp)}(p_2,p_b)u(p_b,\lambda_b),\end{aligned} \quad (2.35)$$

where $s_{ij}=(p_i+p_j)^2$, $p_t=p_a-p_1-p_3$, $p_u=p_4-p_a+p_1$. In the formulas above the $\epsilon_\mu^{(\rho)}$'s denote the polarization vectors of the outgoing ρ^0 mesons. The standard pion propagator $i\Delta^{(\pi)}(k)=i/(k^2-m_\pi^2)$ is used in the calculations. The Reggeized vector meson propagator, denoted by $\tilde{\Delta}_{\mu\nu}^{(V)}(s_{ij},t_i)$ is obtained from (2.16) with the replacement $\Delta_T^{(V)}\to\tilde{\Delta}_T^{(V)}$ from (2.17) and (2.18) and with the relevant s_{ij}, $s_{\rm thr}$, and t_i, the four-momentum transfer squared, in the $p\rho^0$ and $\rho^0\rho^0$ subsystems.

With k',μ and k,ν the four-momentum and vector index of the outgoing ρ^0 and incoming ω meson, respectively, and $k'-k$ the four-momentum of the pion the $\rho\omega\pi$ vertex, including form factor, reads[1]

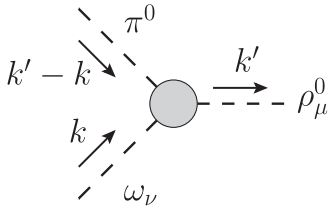

$$i\Gamma_{\mu\nu}^{(\rho\omega\pi)}(k',k)=-i\frac{g_{\rho\omega\pi}}{\sqrt{m_\rho m_\omega}}\varepsilon_{\mu\nu\rho\sigma}k'^\rho k^\sigma F(k'^2,k^2,(k'-k)^2), \tag{2.36}$$

where $g_{\rho\omega\pi}\simeq\pm10$ [37,39,44]. We note that the value of $g_{\rho\omega\pi}=+10$, has been extracted in [39] from the measured $\omega\to\pi^0\gamma$ radiative decay rate and the positive sign from the analysis of pion photoproduction reaction in conjunction with the VMD assumption. In [44] it was found that the data for the reaction $pp\to pp\omega$ strongly favor a negative sign of the coupling constant $g_{\rho\omega\pi}$. In our case, the sign of $g_{\rho\omega\pi}$ does not matter as this coupling occurs twice in the amplitudes (2.34) and (2.35).

We use a factorized ansatz for the form factor

$$F(k'^2,k^2,(k'-k)^2)=F_\rho(k'^2)F_\omega(k^2)F_\pi((k'-k)^2). \tag{2.37}$$

The form factor (2.37) should be normalized as $F(0,m_\omega^2,m_\pi^2)=1$, consistent with the kinematics at which the coupling constant $g_{\rho\omega\pi}$ is determined. This is the $\omega\to\pi^0\gamma$ reaction where ω and π^0 are on shell and the virtual ρ^0 which gives the γ has mass zero. Following [39] we take

$$F_V(t)=\frac{\Lambda_{MV}^2-xm_V^2}{\Lambda_{MV}^2-t}, \tag{2.38}$$

$$F_\pi(t)=\frac{\Lambda_{M\pi}^2-m_\pi^2}{\Lambda_{M\pi}^2-t}, \tag{2.39}$$

where $x=0$ for $V=\rho$ and $x=1$ for $V=\omega$. In this way $F_\rho(t)$ in (2.38) is normalized at $t=0$ and $F_\omega(t)$ at $t=m_\omega^2$. We assume for the cutoff parameters that they are equal to a common value $\Lambda_M\equiv\Lambda_{M\omega}=\Lambda_{M\rho}=\Lambda_{M\pi}$. Following [39] we take $\Lambda_M=1.45$ GeV. Smaller values of the cutoff parameters, $\Lambda_{M\rho}=\Lambda_{M\pi}=1.0$ GeV, were used in [43] (see Table I there). Also a dipole form factor $F_V(t)$ in (2.38) was considered; see [50,51] and Table II of [43].

For the π^0-(anti)proton vertex we have [see (3.4) of [52]]

$$\begin{aligned}i\Gamma^{(\pi pp)}(p',p)&=-i\Gamma^{(\pi\bar{p}\,\bar{p})}(p',p)\\&=-\gamma_5 g_{\pi pp}F_{\pi NN}((p'-p)^2).\end{aligned} \tag{2.40}$$

We take $g_{\pi pp}=\sqrt{4\pi\times14.0}$ and the form factor $F_{\pi NN}(t)$ as in (2.39) with the replacement $\Lambda_{M\pi}\to\Lambda_{\pi NN}$. We take $\Lambda_{\pi NN}=1.0$ GeV; see the discussion in [37,41].

Likewise, the monopole form factor (2.15) in the Vpp vertex (2.12) is assumed with the cutoff parameter Λ_{VNN}. We take $\Lambda_{VNN}=0.9$ GeV and 1.35 GeV in accordance with (C10) and (C7), respectively.

Taking into account the statistical factor $\frac{1}{2}$ due to the identity of the two ρ^0 mesons in (2.32) we get for the amplitude squared

$$\begin{aligned}\frac{1}{2}|\mathcal{M}_{pp\to pp\rho^0\rho^0}|^2&=\frac{1}{2}\frac{1}{4}\sum_{\rm spins}|\mathcal{M}_{\lambda_a\lambda_b\to\lambda_1\lambda_2\lambda_3\lambda_4}|^2\\&=\frac{1}{8}\sum_{\rm spins}(\mathcal{M}_{\lambda_a\lambda_b\to\lambda_1\lambda_2\lambda_3\lambda_4})^*\mathcal{M}_{\lambda_a\lambda_b\to\lambda_1\lambda_2\lambda_3\lambda_4}.\end{aligned} \tag{2.41}$$

Now we discuss the proton-antiproton collisions. Here the amplitudes of the $\rho\rho$ continuum via $\omega\omega$ and $\pi\pi$ fusion can be treated as in (2.34) and (2.35) but with the replacements (2.30) and

$$\begin{aligned}&\bar{u}(p_2,\lambda_2)i\Gamma^{(\pi pp)}(p_2,p_b)u(p_b,\lambda_b)\\&\quad\to\bar{v}(p_b,\lambda_b)i\Gamma^{(\pi\bar{p}\,\bar{p})}(p_2,p_b)v(p_2,\lambda_2)\\&\quad=\bar{u}(p_2,\lambda_2)i\Gamma^{(\pi pp)}(p_2,p_b)u(p_b,\lambda_b),\end{aligned} \tag{2.42}$$

respectively. Using (2.30) and (2.42) we obtain

$$\mathcal{M}^{(\omega\omega\,\text{fusion})}_{p\bar{p}\to p\bar{p}\rho^0\rho^0}=-\mathcal{M}^{(\omega\omega\,\text{fusion})}_{pp\to pp\rho^0\rho^0}, \tag{2.43}$$

$$\mathcal{M}^{(\pi\pi\,\text{fusion})}_{p\bar{p}\to p\bar{p}\rho^0\rho^0}=\mathcal{M}^{(\pi\pi\,\text{fusion})}_{pp\to pp\rho^0\rho^0}. \tag{2.44}$$

As will be discussed in the following, from the $\pi^+\pi^-\pi^+\pi^-$ channel it may be rather difficult to extract

[1]The effective Lagrangian is as given in (1) of [44] taking into account that we use the opposite sign convention for $\varepsilon_{\mu\nu\rho\sigma}$ ($\varepsilon_{0123}=+1$).

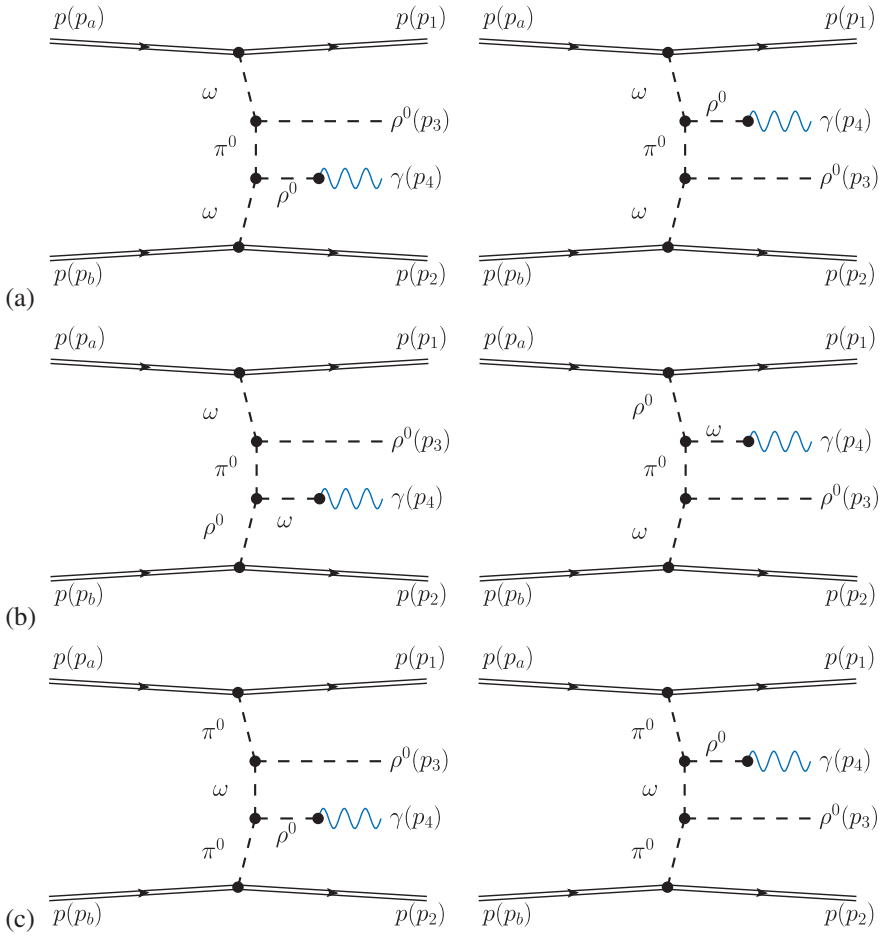

FIG. 3. Diagrams for continuum $\rho^0\gamma$ production: (a) $\omega\omega$ fusion, (b) $\omega\rho$ and $\rho\omega$ fusion, (c) $\pi\pi$ fusion.

the $f_1(1285)$ signal. Another decay channel worth considering is $\rho^0\gamma$.

Therefore, now we discuss the exclusive production of the $\rho^0\gamma$ continuum in proton-proton collisions,

$$p(p_a,\lambda_a)+p(p_b,\lambda_b) \to p(p_1,\lambda_1)+\rho^0(p_3,\lambda_3)+\gamma(p_4,\lambda_4)+p(p_2,\lambda_2) \quad (2.45)$$

with p_4 and $\lambda_4 = \pm 1$ the four-momentum and helicities of the photon.

In order to calculate the amplitude for the reaction (2.45) we use the standard VMD model with the γV couplings as given in (3.23)–(3.25) of [28]. We shall consider the diagrams shown in Fig. 3. The result is as follows:

$$\mathcal{M}^{(\rho\gamma\,\text{continuum})}_{pp\to pp\rho^0\gamma} = \mathcal{M}^{(\omega\omega\,\text{fusion})}_{pp\to pp\rho^0\gamma} + \mathcal{M}^{(\omega\rho\,\text{fusion})}_{pp\to pp\rho^0\gamma} + \mathcal{M}^{(\pi\pi\,\text{fusion})}_{pp\to pp\rho^0\gamma}. \quad (2.46)$$

We could also have $\pi\eta$ and $\pi\sigma$ fusion contributions. For these we have to replace in the left (right) diagram in Fig. 3(c) the lower (upper) particles (π^0,ρ^0) by (η,ω) or (σ,ω), respectively. Discussing first $\pi\eta$ fusion we note that the couplings ηpp and $\omega\omega\eta$ are smaller than those of $\pi^0 pp$ and $\rho\omega\pi$ [37]. In addition, the η exchange is suppressed relative to the π^0 exchange because of the heavier mass occurring in the propagator. Another mechanism is the $\pi\sigma$ fusion involving the σpp and $\sigma\omega\omega$ vertices. However, here $g_{\sigma\omega\omega} \sim 0.5$ [37] is extremely small. Moreover, the $\omega\to\gamma$ transition coupling is much smaller than the $\rho\to\gamma$ one; see (A5). Therefore, we neglect the $\pi\eta$ and $\pi\sigma$ contributions in our considerations.

Thus, we are left with the $(\omega+\rho^0)-\pi^0-\omega$, $\omega-\pi^0-(\omega+\rho^0)$, and $\pi^0-\omega-\pi^0$ contributions, which we shall treat in a way similar to (2.34) and (2.35). As an example, the $\mathcal{M}^{(\omega\omega\,\text{fusion})}_{pp\to pp\rho^0\gamma}$ amplitude can be written as in (2.34) with the following replacement:

$$\epsilon^{(\rho)\rho_4}(\lambda_4=0,\pm1) \to \frac{e}{\gamma_\rho}\epsilon^{(\gamma)\rho_4}(\lambda_4=\pm1). \quad (2.47)$$

In the case of the diagrams with the $\omega\to\gamma$ transition, the outgoing ω has four-momentum squared $p^2=0$. Since nothing is known about the form factor at the $\rho\omega\pi$ vertex where both the π^0 and ρ^0 are off their mass-shell, we

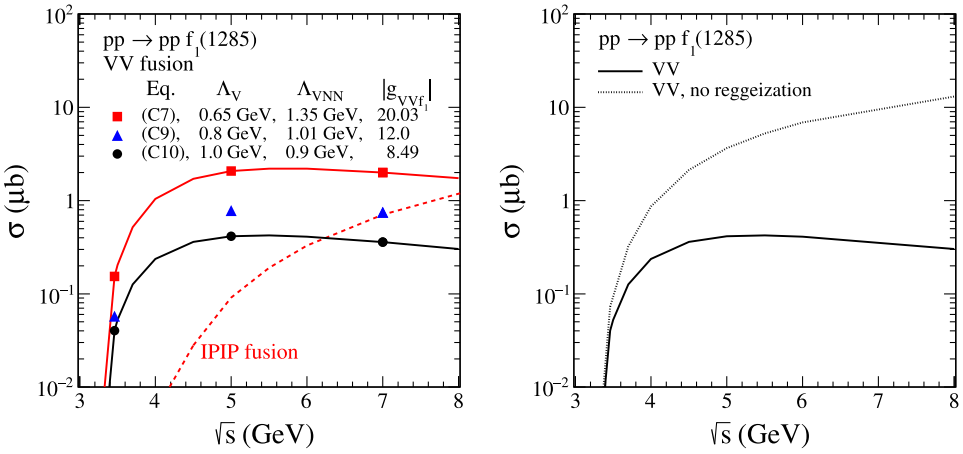

FIG. 4. Integrated cross section for the $pp \to ppf_1(1285)$ reaction as a function of collision energy $\sqrt{s}$ for $VV \to f_1(1285)$ fusion with different parameters from Eqs. (C7), (C9), and (C10). We show also the Pomeron-Pomeron fusion mechanism (red dashed line). In the right panel, the solid line is for the parameters of (C10) and the Reggeized propagators $\tilde{\Delta}_T^{(V)}$, the dotted line corresponds to the result for the standard vector-meson propagators $\Delta_T^{(V)}$, i.e., without Reggeization; see (2.17)–(2.19). No rescattering effects are included here.

assume in (2.36) the form factor (2.37) as $F(m_\rho^2, 0, m_\pi^2) = 1$ which is consistent with (2.38) and (2.39).

The $\rho\gamma$-continuum processes in proton-antiproton collisions can be treated in a completely analogous way to the $\rho\gamma$-continuum processes in proton-proton collisions but with the appropriate replacements given by (2.30) and (2.42).

III. NUMERICAL RESULTS

We start by showing the integrated cross section for the exclusive reaction $pp \to ppf_1(1285)$ as a function of collision energy $\sqrt{s}$ from threshold to 8 GeV. Note that due to (2.31) the cross sections and distributions for the VV-fusion mechanism are equal for pp and $p\bar{p}$ scattering for the same kinematical values.

In Fig. 4 we show results for the VV-fusion contributions ($V = \rho, \omega$) for different parameters given by (C7), (C9) and (C10) in Appendix C. We assume $g_{\omega\omega f_1} = g_{\rho\rho f_1} \equiv g_{VVf_1}$; see (A9). The cross section first rises from the threshold $\sqrt{s_{\rm thr}} = 2m_p + m_{f_1}$ to $\sqrt{s} \approx 5$ GeV (PANDA energy range), where it starts to decrease toward higher energies. The region of fast growth of the cross section is related to the fast opening of the phase space, while the Reggeization is responsible for the decreasing part. Without the Reggeization the cross section would continue to grow. The Reggeization, calculated according to (2.17)–(2.19), reduces the cross section by a factor of 1.8 already for the HADES c.m. energy $\sqrt{s} = 3.46$ GeV. For comparison we also show the high-energy contribution of the $\mathbb{PP} \to f_1(1285)$ fusion (see the red dashed line) with parameters fixed in [27]; see Eq. (3.7) there. As mentioned in Appendix D of [27], due to the possible influence of subleading Reggeon exchanges, the $\mathbb{PP}$-fusion contribution should be regarded rather as an upper limit.

At near-threshold energies one should consider final state interactions (FSI) between the two produced protons; see e.g., [37,51]. But the effect is sizeable only for extremely small excess energies of tens of MeV: $Q_{\rm exc} = \sqrt{s} - \sqrt{s_{\rm thr}}$. In our case, we have $Q_{\rm exc} > 300$ MeV and this FSI effect can be neglected.

We remind the reader that our calculation of the VV-fusion processes should only be applied at energies $\sqrt{s} \lesssim 8$ GeV. In the intermediate energy range also other processes like $f_{2\mathbb{R}} f_{2\mathbb{R}}$ fusion must be considered; see the discussion in Appendix D of [27].

The salient feature of the results shown in Fig. 4 is the high sensitivity of the VV-fusion cross section to the different sets of parameters. In our procedure of extracting the coupling constant g_{VVf_1} and the form-factor cutoff parameters from the CLAS data [see Appendices B and C] the dominant sensitivity is on g_{VVf_1}, not on the form factors. Also the form of Reggeization used in our model, according to (2.17)–(2.21), affects the size of the cross section. With the parameter values of (C10) we get

$$\text{for } \sqrt{s} = 3.46 \text{ GeV}: \ \sigma_{pp\to ppf_1} = 40.22 \text{ nb}, \tag{3.1}$$

$$\text{for } \sqrt{s} = 5.0 \text{ GeV}: \ \sigma_{p\bar{p}\to p\bar{p}f_1} = 413.85 \text{ nb}. \tag{3.2}$$

With the parameter values of (C7) we get

$$\text{for } \sqrt{s} = 3.46 \text{ GeV}: \ \sigma_{pp\to ppf_1} = 153.52 \text{ nb}, \tag{3.3}$$

$$\text{for } \sqrt{s} = 5.0 \text{ GeV}: \ \sigma_{p\bar{p}\to p\bar{p}f_1} = 2071.43 \text{ nb}. \tag{3.4}$$

As mentioned above, the different numbers in (3.1) and (3.2) compared to (3.3) and (3.4) reflect mainly the different couplings g_{VVf_1}. Indeed, from (3.3) and (3.1) we get for the cross section ratio 3.8, from (3.4) and (3.2)

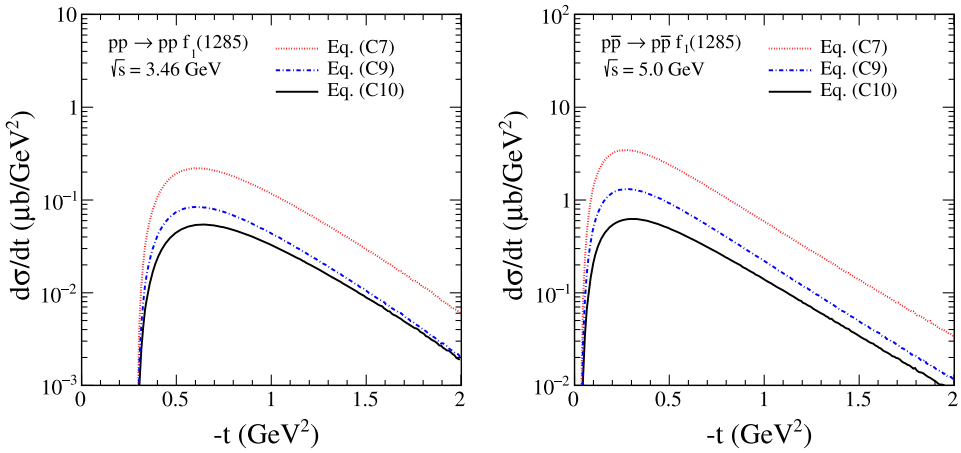

FIG. 5. Distributions in $-t$ for $\sqrt{s} = 3.46$ and 5.0 GeV. Results for different parameters (C7), (C9), and (C10) are shown. In the calculations we take the Vpp coupling constants from (2.13).

we get 5.0, and from (C7) and (C10) we get for the ratio of the coupling constants squared 5.6, not far from the two numbers above.

In Fig. 5 we show the distributions in the four-momentum transfer squared from one of the proton vertices [we have $t = t_1$ or t_2, cf. (2.2)] for $\sqrt{s} = 3.46$ GeV (HADES) and 5.0 GeV (PANDA). One can observe that $d\sigma/dt$ decreases rapidly at forward scattering $|t| \to |t|_{\rm min}$, where $|t|_{\rm min} \simeq 0.3$ GeV^2 at $\sqrt{s} = 3.46$ GeV. At near threshold energy the values of small $|t_1|$ and $|t_2|$ are not accessible

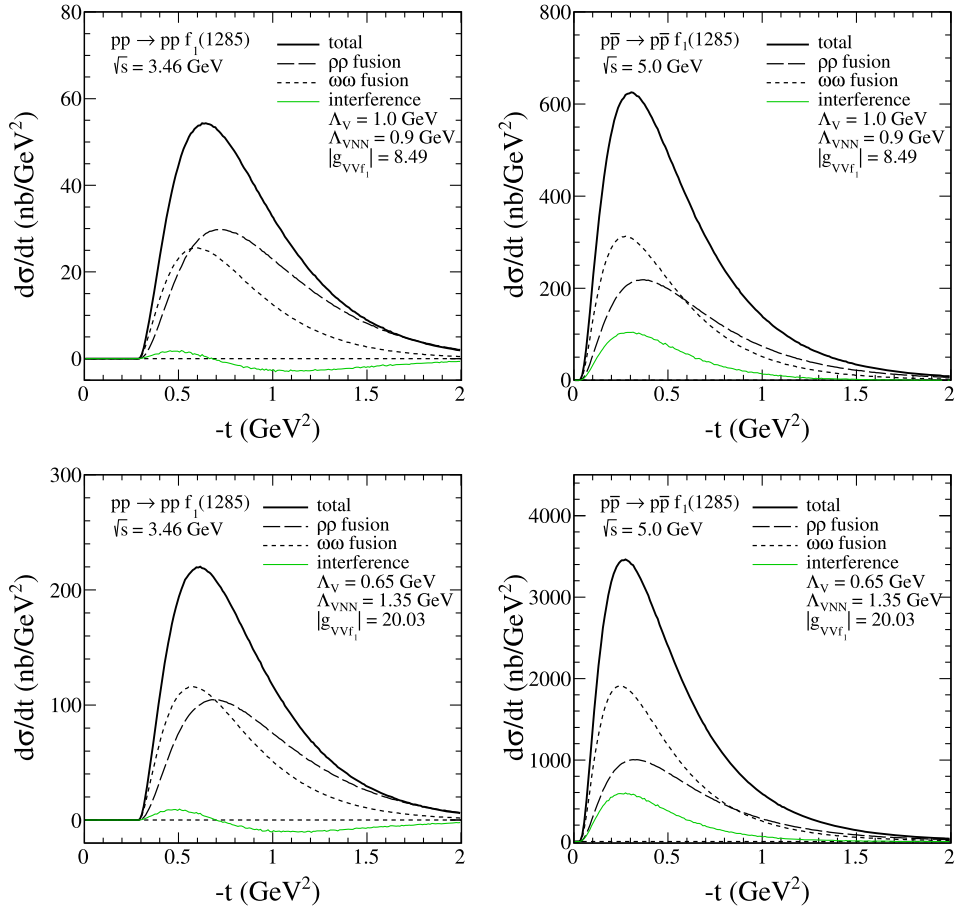

FIG. 6. Distributions in $-t$ for $\sqrt{s} = 3.46$ (left panels) and 5.0 GeV (right panels). In the calculations we take the parameters given in (2.13), (C10) and (C7). The results shown on the top panels correspond to (C10) and those on the bottom panels are for (C7).

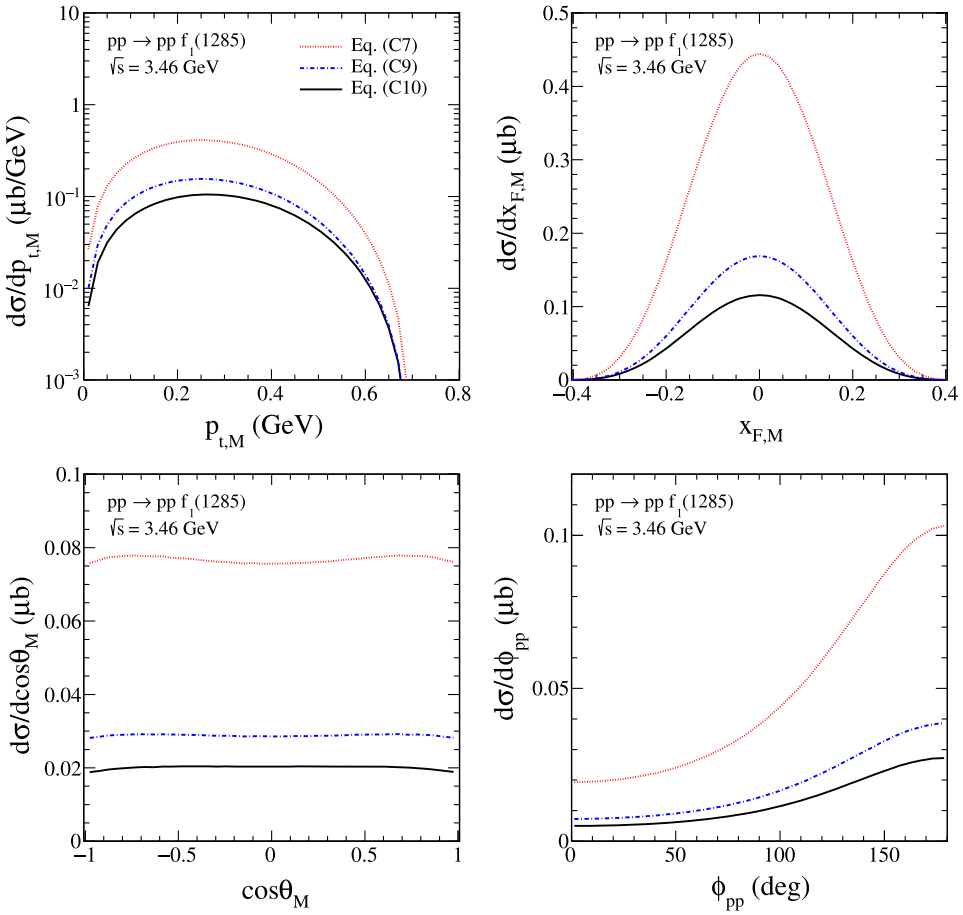

FIG. 7. Several differential distributions for the reaction $pp \to ppf_1(1285)$ at $\sqrt{s} = 3.46$ GeV relevant for the HADES experiment. The meaning of the lines is as in Fig. 5 (left panel).

kinematically. The maximum of $d\sigma/dt$ appears at $-t_{1,2} \simeq 0.65$ GeV^2 for the parameter values of (C10) and at $-t_{1,2} \simeq 0.77$ GeV^2 for those of (C11). The close-to-threshold production of the f_1 meson, therefore, probes corresponding form factors, (2.10), (2.11) and (2.15), at relatively large values of $|t_1|$ and $|t_2|$, far from their on mass-shell values at $t_{1,2} = m_V^2$ where they were normalized. Thus, the VV-fusion cross section is very sensitive to the choice of the form factors. Therefore the HADES and PANDA experiments have a good opportunity to study physics of large four-momentum transfer squared.

In Fig. 6 we present the contributions for the $\omega\omega$- and $\rho\rho$-fusion processes separately and their coherent sum (total). The interference term is shown also (see the green solid line). Both processes play roughly similar role. For large values of $|t_1|$ and $|t_2|$, in spite of $g_{\rho pp} < g_{\omega pp}$ (2.13), the spin-flip term of the ρ^0-proton coupling is important. For $\sqrt{s} = 5.0$ GeV the $\omega\omega$-fusion contribution is the dominant process for $|t_{1,2}| \lesssim 0.5$ GeV^2. There one can see also a large constructive interference effect.

In Figs. 7 and 8 we show several differential distributions for the reaction $pp \to ppf_1(1285)$ for $\sqrt{s} = 3.46$ GeV relevant for the HADES experiment and for the reaction $p\bar{p} \to p\bar{p}f_1(1285)$ for $\sqrt{s} = 5.0$ GeV relevant for the PANDA experiment, respectively. We show the distributions in the transverse momentum of the $f_1(1285)$ meson, in $x_{F,M}$, the Feynman variable of the meson, in the $\cos\theta_M$ where θ_M is the angle between k and p_a in the c.m. frame, and in ϕ_{pp}, the azimuthal angle between the transverse momentum vectors $p_{t,1}$, $p_{t,2}$ of the outgoing nucleons in the c.m. frame. We predict a strong preference for the outgoing nucleons to be produced with their transverse momenta being back-to-back ($\phi_{pp} \approx \pi$). The distributions in $\cos\theta_M$ for the energies $\sqrt{s} = 3.46$ GeV and $\sqrt{s} = 5.0$ GeV have a different shape. This is explained in Fig. 9. One can observe from Figs. 6 and 9 that the $\omega\omega$- and $\rho\rho$-fusion processes have different kinematic dependences. With increasing energy $\sqrt{s}$ the averages of $|t_1|$ and $|t_2|$ decrease (damping by form factors), hence the $\omega\omega$ contribution becomes more important.

Now we turn to the $pp \to pp(f_1(1285) \to \rho^0\gamma)$ reaction and the discussion of background processes.

In Fig. 10 we show the invariant mass distributions of the $\rho^0\gamma$ system at $\sqrt{s} = 3.46$ GeV (HADES experiment) and at

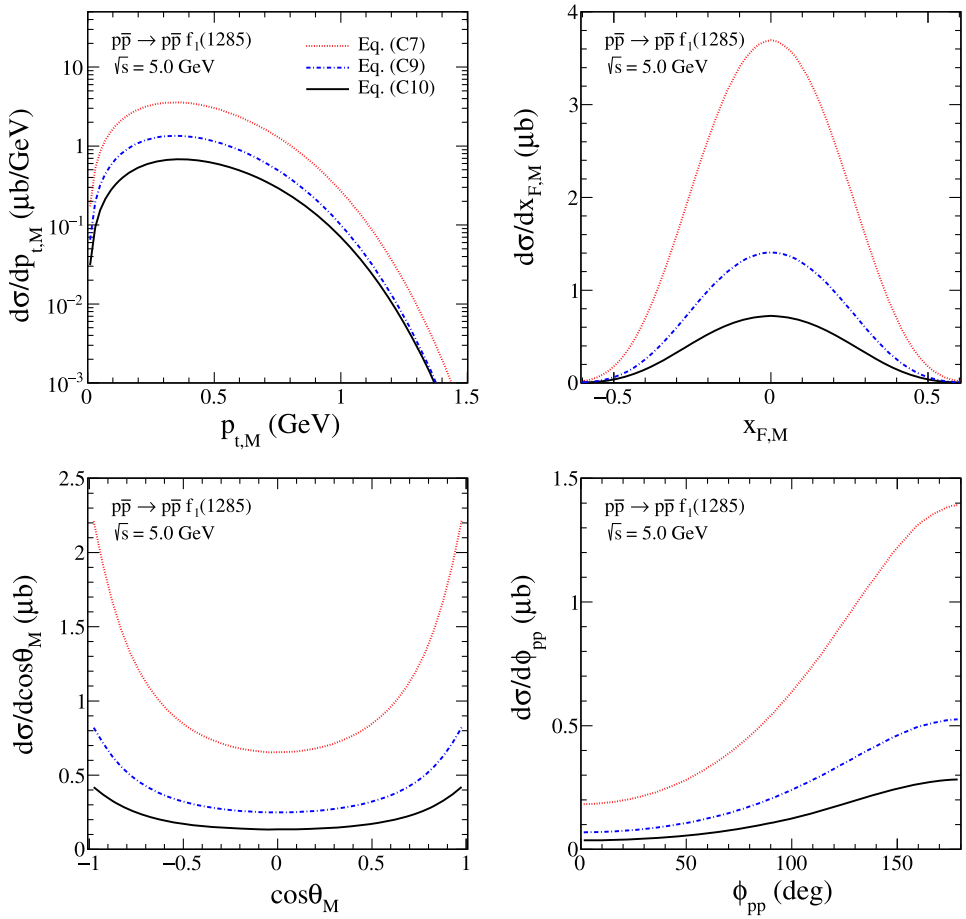

FIG. 8. Several differential distributions for the reaction $p\bar{p} \to p\bar{p}f_1(1285)$ at $\sqrt{s} = 5.0$ GeV relevant for the PANDA experiment. The meaning of the lines is as in Fig. 5 (right panel).

$\sqrt{s} = 5.0$ GeV (PANDA experiment). The red solid line represents the $f_1(1285)$ signal via the $\rho\rho$ and $\omega\omega$ fusion processes while the other lines represent the background corresponding to the processes via the VV ($\omega\omega$, $\rho\omega$) and $\pi\pi$ fusion shown by the diagrams of Fig. 3. Results for the two sets of parameters (C10) and (C7) which correspond to the top and bottom panels, respectively, are shown. In the f_1 meson propagator (2.25) we take $\Gamma_{f_1} = 18.4$ MeV

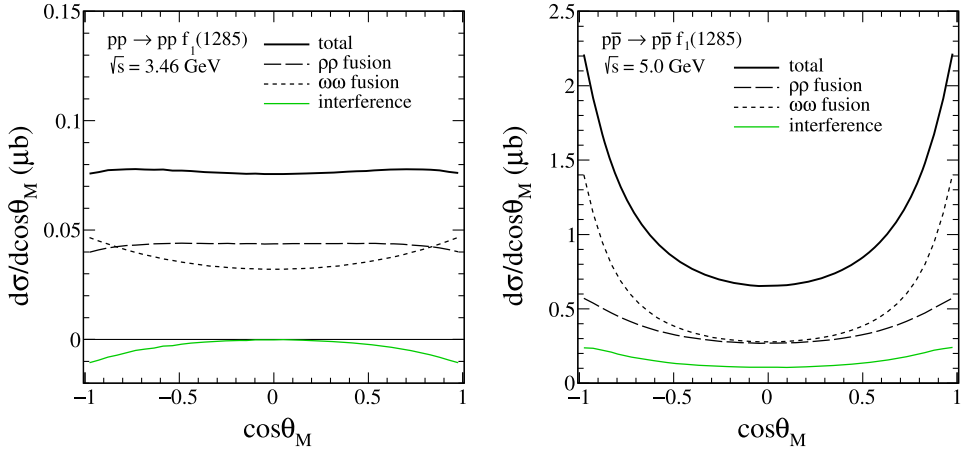

FIG. 9. Distributions in $\cos\theta_M$ for $\sqrt{s} = 3.46$ GeV (left panel) and $\sqrt{s} = 5.0$ GeV (right panel). The meaning of the lines is as in the bottom panels of Fig. 6. Results for the parameter values of (2.13) and (C7) are shown.

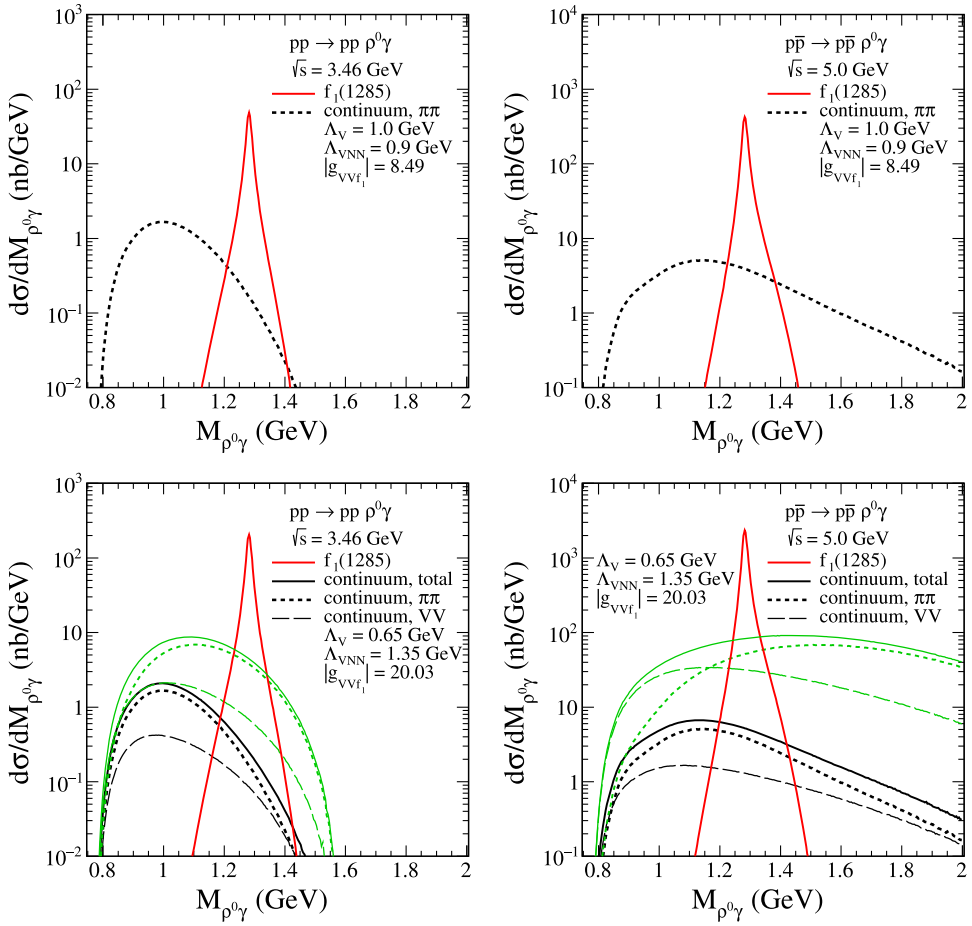

FIG. 10. Invariant mass distributions of the $\rho^0\gamma$ system for the HADES experiment (left panels) and the PANDA experiment (right panels). The $VV \to f_1(1285)$ resonance term and continuum processes via $\pi\pi$ and VV fusion are shown. Results in the top panels are for the parameter values of (C10), while in the bottom panels for those of (C7). In the calculations we take $\Lambda_M = 1.45$ GeV and $\Lambda_{\pi NN} = 1.0$ GeV. In the bottom panels, the green lines (upper lines for the same type) correspond to the continuum processes without Reggeization.

measured in the CLAS experiment; see (2.28). For the set of parameters (C10) the VV-continuum contribution, due to the small value of Λ_{VNN}, turns out to be negligible. The situation changes when we use the parameter set of (C7). But still the $\pi\pi$-continuum contribution is larger than the VV-continuum contribution. In both cases the $f_1(1285)$ resonance is clearly visible, even without the Reggeization effects in the continuum processes. This result makes us rather optimistic that an experimental study of the f_1 in the $\rho^0\gamma$ decay channel should be possible.

In our calculations we find practically no interference effects between the $\pi\pi$ and VV fusion contributions in the continuum. For our exploratory study we have neglected interference effects between the background $\rho^0\gamma$ and the signal $f_1 \to \rho^0\gamma$ processes. We have also neglected the background processes due to bremsstrahlung of γ and ρ^0 from the nucleon lines. For an analysis of real data these effects should be included or at least estimated. But this goes beyond the scope of our present paper.

Now we wish to discuss the integrated cross sections for the reactions $pp \to pp(f_1 \to \rho^0\gamma)$ and $p\bar{p} \to p\bar{p}(f_1 \to \rho^0\gamma)$ treated with exact $2 \to 4$ kinematics. In our calculation we took into account the Reggeization effects according to (2.17)–(2.21) and the replacements given in (2.23). We consider two sets of parameters, (C10) and (C7), extracted from the CLAS data. With the parameter values of (C10) we get

$$\text{for } \sqrt{s} = 3.46 \text{ GeV}: \ \sigma_{pp\to pp(f_1\to\rho^0\gamma)} = 1.26 \text{ nb}, \tag{3.5}$$

$$\text{for } \sqrt{s} = 5.0 \text{ GeV}: \ \sigma_{p\bar{p}\to p\bar{p}(f_1\to\rho^0\gamma)} = 11.45 \text{ nb}. \tag{3.6}$$

With the parameter values of (C7) we get

$$\text{for } \sqrt{s} = 3.46 \text{ GeV}: \ \sigma_{pp\to pp(f_1\to\rho^0\gamma)} = 5.38 \text{ nb}, \tag{3.7}$$

$$\text{for } \sqrt{s} = 5.0 \text{ GeV}: \ \sigma_{p\bar{p}\to p\bar{p}(f_1\to\rho^0\gamma)} = 62.86 \text{ nb}. \tag{3.8}$$

The results (3.5)–(3.8) are for $\Gamma_{f_1} = 18.4$ MeV; see (2.28). We have checked, that if we take for the cutoff parameter $\Lambda_{f_1} = 1.2$ GeV in (2.24) that the cross sections will increase slightly, by about 1.6%.

Now we compare the above results with those estimated as

$$\sigma_{pp\to pp(f_1\to\rho^0\gamma)} = \sigma_{pp\to ppf_1} \times \mathcal{BR}(f_1(1285)\to\rho^0\gamma) \quad (3.9)$$

with the corresponding values of the $2\to 3$ cross sections from (3.1)–(3.4) and $\mathcal{BR}(f_1\to\rho^0\gamma)$ from CLAS (B8). For the parameter set (C10) we get

$$\text{for } \sqrt{s} = 3.46\,\text{GeV}: \sigma_{pp\to pp(f_1\to\rho^0\gamma)} = 1.00^{+0.28}_{-0.36}\,\text{nb}, \quad (3.10)$$

$$\text{for } \sqrt{s} = 5.0\,\text{GeV}: \sigma_{p\bar{p}\to p\bar{p}(f_1\to\rho^0\gamma)} = 10.35^{+2.89}_{-3.72}\,\text{nb}. \quad (3.11)$$

For the parameter set (C7) we get

$$\text{for } \sqrt{s} = 3.46\,\text{GeV}: \sigma_{pp\to pp(f_1\to\rho^0\gamma)} = 3.84^{+1.08}_{-1.38}\,\text{nb}, \quad (3.12)$$

$$\text{for } \sqrt{s} = 5.0\,\text{GeV}: \sigma_{p\bar{p}\to p\bar{p}(f_1\to\rho^0\gamma)} = 51.79^{+14.50}_{-18.64}\,\text{nb}. \quad (3.13)$$

The errors in (3.10)–(3.13) come from the uncertainty of $\mathcal{BR}(f_1\to\rho^0\gamma)$; see (B8). The results (3.5)–(3.8) are larger than the corresponding central values of (3.10)–(3.13).

For $p\bar{p}$ at $\sqrt{s} = 5.0$ GeV we obtain about 10 times larger cross section than for pp at $\sqrt{s} = 3.46$ GeV; see (3.8) and (3.7). respectively. Thus we predict a large cross section for the exclusive axial-vector $f_1(1285)$ production compared to the continuum processes considered in the $\rho^0\gamma$ channel.

In Table I we have collected integrated cross sections in nb for the continuum processes considered. These numbers were obtained for $g_{\rho\omega\pi} = 10.0$, $\Lambda_M = 1.45$ GeV in (2.36)–(2.39), $\Lambda_{VNN} = 1.35$ GeV in (2.15), and $\Lambda_{\pi NN} = 1.0$ GeV in (2.40). The Reggeization effects were included. We can observe very small numbers for the production of $\rho^0\rho^0$ at $\sqrt{s} = 3.46$ GeV which is caused by the threshold behavior of the process (the assumption of a fixed ρ^0-meson mass of $m_\rho = 0.775$ GeV in the calculation) and limited phase space.

Now we compare the cross section for the $\rho\rho$ continuum from Table I to the cross section for the $f_1(1285)$ signal according to

$$\sigma_{pp\to pp(f_1\to 2\pi^+2\pi^-)} = \sigma_{pp\to ppf_1} \times \mathcal{BR}(f_1\to 2\pi^+2\pi^-) \quad (3.14)$$

with $\sigma_{pp\to ppf_1}$ from Fig. 4 and a branching ratio

$$\mathcal{BR}(f_1(1285)\to 2\pi^+2\pi^-) = (10.9\pm 0.6)\% \quad (3.15)$$

from [47]. Taking into account the values of $\sigma_{pp\to ppf_1}$ in (3.14) that correspond to (C10) we get

TABLE I. The integrated cross sections in nb for the continuum processes in proton-(anti)proton collisions. We show results for the VV- and $\pi\pi$-fusion contributions separately and for their coherent sum ("total").

		σ (nb)		
Reaction	$\sqrt{s}$ (GeV)	VV fusion	$\pi\pi$ fusion	Total
$pp\to pp\rho^0\rho^0$	3.46	0.6×10^{-3}	6.7×10^{-3}	7.3×10^{-3}
$p\bar{p}\to p\bar{p}\rho^0\rho^0$	5.0	156.24	1823.25	1979.50
$pp\to pp\rho^0\gamma$	3.46	0.13	0.45	0.58
$p\bar{p}\to p\bar{p}\rho^0\gamma$	5.0	1.06	2.49	3.56

$$\text{for } \sqrt{s} = 3.46\,\text{GeV}: \sigma_{pp\to pp(f_1\to 2\pi^+2\pi^-)} = 4.38\,\text{nb}, \quad (3.16)$$

$$\text{for } \sqrt{s} = 5.0\,\text{GeV}: \sigma_{p\bar{p}\to p\bar{p}(f_1\to 2\pi^+2\pi^-)} = 45.11\,\text{nb}. \quad (3.17)$$

With (C7) we get

$$\text{for } \sqrt{s} = 3.46\,\text{GeV}: \sigma_{pp\to pp(f_1\to 2\pi^+2\pi^-)} = 16.73\,\text{nb}, \quad (3.18)$$

$$\text{for } \sqrt{s} = 5.0\,\text{GeV}: \sigma_{p\bar{p}\to p\bar{p}(f_1\to 2\pi^+2\pi^-)} = 225.79\,\text{nb}. \quad (3.19)$$

These roughly estimated results show that, for the cases treated here, the background processes considered in the $\rho^0\rho^0$ channel (see Table I) can be important only for $\sqrt{s} = 5.0$ GeV in the $p\bar{p}$ case.

The reaction $pp\to pp\rho^0\rho^0$ is treated technically as a $2\to 4$ process. A better approach would be to consider the $pp\to pp\pi^+\pi^-\pi^+\pi^-$ reaction, as a $2\to 6$ process. This is however beyond the scope of the present study. In addition, as will be discussed in the following, the background for the $pp\to pp\pi^+\pi^-\pi^+\pi^-$ reaction measured long ago by the bubble chamber experiment [53] was found to be much larger than the result for the continuum terms ("total") presented in Table I.

IV. HADES AND PANDA EXPERIMENTS

The HADES (High Acceptance Dielectron Spectrometer) is a magnetic spectrometer located at the SIS18 accelerator in the Facility for Antiproton and Ion Research (FAIR) in Darmstadt (Germany) [54]. It is a versatile detector allowing measurement of charged hadrons (pions, kaons and protons), leptons (electrons and positrons) originating from various reactions on fixed proton or nuclear targets in the energy regime of a few $A\cdot$ GeV. The spectrometer covers the polar angle region $18° < \theta < 80°$ and features almost complete azimuthal coverage with respect to the beam axis. The detector has been recently upgraded by a large area electromagnetic calorimeter and a forward detector (for a recent review see [55]) extending the coverage to very forward region ($0.5° < \theta < 7.5°$). These upgrades allow us to measure hadron decays involving photons and significantly improve acceptance for protons and hyperons which at these energies are emitted to large extent in forward directions.

The spectrometer is specialized for electron-positron pair detection but it also provides excellent hadron (pion, kaon, proton)-identification capabilities. It has a low material budget and consequently features an excellent invariant mass resolution for electron-positron pairs of $\Delta M/M \approx 2.5\%$ in the $\rho/\omega/\phi$ vector meson mass region.

The PANDA (antiProton ANnihilations at DArmstadt) detector is currently under construction at FAIR. PANDA will utilize a beam of antiprotons, provided by the High Energy Storage Ring (HESR), and with its almost full solid-angle coverage will be a detector for precise measurements in hadron physics. HESR will deliver antiprotons with momenta from 1.5 GeV/c up to 15 GeV/c (which corresponds to $\sqrt{s} \simeq 2.25$–5.47 GeV) impinging on a cluster jet or pallet proton target placed in PANDA. The scientific programme of PANDA is very broad and includes charmonium and hyperon spectroscopy, elastic proton form-factor measurements, searches of exotic states and studies of in-medium hadron properties (for a recent review of stage-one experiments see [56]).

The luminosity of both detectors are comparable and are at the level of $L = 10^{31}$ cm$^{-2}s^{-1}$ (after first years of operation and completion of the detector PANDA will increase it by one order of magnitude).

For the count rate estimates and signal to background considerations for the f_1 meson production we will use the properties of the HADES detector. This presents a "worst case" scenario. As it was shown in previous sections cross sections for the meson production in proton-proton interactions are about a factor 10 lower than for the proton-antiproton case. Furthermore, the PANDA detector features also larger acceptance for the reaction of multiparticle finals and presents better opportunities for the studies discussed in this work. On the other hand HADES will measure proton-proton reactions at the c.m. energy $\sqrt{s} = 3.46$ GeV (proton beam energy $E_{\rm kin} = 4.5$ GeV) already in 2021. Hence it will provide first valuable experimental results to verify our model predictions.

A. Simulation for $2\pi^+2\pi^-$ and $\pi^+\pi^-\eta$ decay channels

We have considered production of the $f_1(1285)$ meson in proton-proton reactions and its decay into final states with four charged pions reconstructed in the HADES detector. For the f_1 production cross section we have assumed $\sigma_{f_1} = 150$ nb [estimate using the C7 parameter set; see (C7) and (3.3)].

Two reaction channels were simulated:

$$p + p \to p + p + f_1(\to 2\pi^+2\pi^-) \quad \text{with}$$
$$\mathcal{BR}(f_1(1285) \to 2\pi^+2\pi^-) = 10.9\%, \tag{4.1}$$

$$p + p \to p + p + f_1(\to \pi^+\pi^-\eta) \quad \text{with}$$
$$\mathcal{BR}(f_1(1285) \to \pi^+\pi^-\eta) = 35\%. \tag{4.2}$$

In the second case the η meson is reconstructed via the $\eta \to \pi^+\pi^-\pi^0$ decay channel, hence the final state has also four charged pions. The neutral pion from the η decay can be reconstructed via missing mass technique or via two photon decay. However, the latter case has smaller total reconstruction efficiency (see below for details).

The $f_1(1285)$ meson decay into four charged pions has been simulated using the PLUTO event generator [57–59]. For the meson reconstruction four pions from the decay and at least one final state proton have been demanded in the analysis to establish exclusive channel identification. The HADES acceptance and reconstruction efficiencies for protons and pions have been parametrized as a function of the polar and azimuthal angles and the momentum. Furthermore, a momentum resolution $\Delta p/p = 2\%$ of the spectrometer for charged tracks has been taken into account in the simulation, as described in [54].

For the $pp \to pp2\pi^+2\pi^-$ reaction a total cross section $\sigma_{\rm back} = (227 \pm 23)$ μb has been measured; see Table I of [53]. This reaction was measured in [53] at slightly higher energies $E_{\rm kin} = 4.64$ GeV (corresponding to proton beam momentum $P = 5.5$ GeV/c or $\sqrt{s} \simeq 3.5$ GeV).[2]

We tried to understand the large background in the $\pi^+\pi^-\pi^+\pi^-$ channel. We analysed a few contributions due to double nucleon excitations. We considered the following processes:

$$pp \to N(1440)N(1440) \quad \text{via } \pi^0, \sigma, \tag{4.3}$$
$$pp \to N(1440)N(1535) \quad \text{via } \pi^0, \tag{4.4}$$
$$pp \to N(1535)N(1535) \quad \text{via } \pi^0, \eta, \rho^0. \tag{4.5}$$

Both resonances have considerable branching fraction to the $N\pi\pi$ channel and the $N(1535)$ to the $N\eta$ channel; see PDG [47]. In our evaluation (estimation) we used effective Lagrangians and relevant parameters from [60]. These parameters were found in [60] to describe the total cross section for the $pp \to pn\pi^+$ reaction measured in the close-to-threshold region. The coupling constants and the cutoff parameters in the monopole form factors used in the calculation are the following ones:

$$g^2_{N(1440)N\sigma}/4\pi = 3.20, \qquad \Lambda_{N(1440)N\sigma} = 1.1 \text{ GeV},$$
$$g^2_{N(1440)N\pi}/4\pi = 0.51, \qquad \Lambda_{N(1440)N\pi} = 1.3 \text{ GeV},$$
$$g^2_{N(1535)N\pi}/4\pi = 0.037, \qquad \Lambda_{N(1535)N\pi} = 1.3 \text{ GeV},$$
$$g^2_{N(1535)N\eta}/4\pi = 0.34, \qquad \Lambda_{N(1535)N\eta} = 1.3 \text{ GeV},$$
$$g^2_{N(1535)N\rho}/4\pi = 0.097, \qquad \Lambda_{N(1535)N\rho} = 1.3 \text{ GeV}. \tag{4.6}$$

[2]In [53] a four-pion invariant-mass histogram was shown for the $pp \to pp2\pi^+2\pi^-$ reaction [see Fig. 28(a) therein]. No attempt has been made to analyse this channel there and only an upper limit on the resonance (there $f^*(1250) \to 2\pi^+2\pi^-$) production cross section, $\sigma < 15$ μb, was estimated.

TABLE II. Contributions and cross sections used in the simulations of the $pp \to pp2\pi^+2\pi^-\pi^0$ reaction.

Contribution	Cross section (μb)	Discussion
(1) $pp \to pp\pi^+\pi^-\pi^+\pi^-\pi^0$	88	$\sigma = (88 \pm 14)$ μb [53], $P = 5.5$ GeV/c
(2) $pp \to pp\pi^+\pi^-\eta(\to \pi^+\pi^-\pi^0)$	0.18	estimates via two N^* resonances, see (4.4) and (4.5)
(3) $pp \to pp\pi^+\pi^-\omega(\to \pi^+\pi^-\pi^0)$	0.07	$\sigma = (0.09 \pm 0.03)$ μb [70] for $pp \to pp\pi^+\pi^-\omega$ at $P = 6.92$ GeV/c
(4) $pp \to ppf_1[\to \pi^+\pi^-\eta(\to \pi^+\pi^-\pi^0)]$	0.012	$\sigma = (3.2 - 12.4)$ nb, see (3.1) and (3.3)

Similar values were also taken in [61] for the $pn \to d\phi$ reaction. To describe the total cross sections of the $pN \to NN\pi\pi$ and $\bar{p}N \to \bar{N}N\pi\pi$ reactions measured in the near-threshold region the cutoff parameters $\Lambda_{N^*NM} = 1.0$ GeV were assumed in [62,63]. Therefore, our estimates for the reactions (4.3)–(4.5) with the parameters given in (4.6) should be regarded rather as an upper limit.

There is a question about the role of the η' exchange in the reaction (4.5). For example, in [64] subthreshold resonance-dominance of the $N(1535)$ was assumed with $g^2_{N(1535)N\eta'}/4\pi = 1.1$ to describe both the $\pi N \to \eta' N$ and $NN \to NN\eta'$ cross section data. However, it was shown in [65] that the $N(1535)$ contribution is not necessary in these processes (see Figs. 9–14 of [65]) or, at least, its significant role (significant coupling strength of $N(1535) \to \eta' N$ used in [64,66]) was precluded.

For energy $\sqrt{s} = 3.5$ GeV we get the cross section for the $pp \to N(1440)N(1440)$ reaction of the order of 0.8 mb. With the input from [67–69], $g^2_{N(1440)N\sigma}/4\pi = 1.33$ and $\Lambda_{N(1440)N\sigma} = 1.7$ GeV, we get even smaller cross section by about 30%. For the $pp \to N(1440)N(1535)$ reaction we get the cross section of 10 μb and for the $pp \to N(1535)N(1535)$ reaction about 7 μb. So we conclude that the double excitation of the $N(1440)$ resonances via the σ-meson exchange is probably the dominant mechanism of this type in the $pp \to pp2\pi^+2\pi^-$ reaction. This is due to the large $N(1440)N\sigma$ coupling. Taking $\mathcal{BR}(N(1440) \to p\pi^+\pi^-) = 0.1$ we get $\sigma_{pp\to N^*N^*\to pp2\pi^+2\pi^-} \simeq 80$ μb. This background is much higher than that for the $\omega\omega$- and $\pi\pi$-fusion mechanisms considered in Sec. III; see Table I.

The background channel was simulated assuming multipion production via two intermediate charged baryon resonances, each of them decaying into two pion final states. Since the exact production mechanism is not known we have assumed production of two $N(1440)$. We take the total cross section for the background in the four pion channel to be $\sigma^{4\pi}_{\rm back} = 227$ μb [53]. For the signal we take $\sigma^{4\pi}_{f_1} = \sigma_{f_1} \times \mathcal{BR}(f_1(1285) \to 2\pi^+2\pi^-) = 16$ nb [see (3.18)]. A total reconstruction efficiency $\epsilon = 2\%$ for the f_1 decay in four charged pions has been estimated and the signal is hardly visible on the top of the background. We conclude that it will be difficult to see a peak on the four-pion continuum without additional cuts.

Now we wish to consider the $pp \to pp\pi^+\pi^-\pi^+\pi^-\pi^0$ reaction. In Table II we have collected the cross sections which we use in the simulations. We take the total cross section for the continuum background in the five pion channel to be $\sigma^{5\pi}_{\rm back} = 88$ μb [53], which seems to be rather an upper limit for the background. Taking into account both processes (4.4) and (4.5) we estimate the cross section in the $pp\pi^+\pi^-\eta$ final state of the order of 0.8 μb to be compared to 53 nb for the signal $pp \to ppf_1(\to \pi^+\pi^-\eta)$. We include $\mathcal{BR}(\eta \to \pi^+\pi^-\pi^0) = 0.23$ to get the $pp\pi^+\pi^-\pi^+\pi^-\pi^0$ final state. For the $pp \to pp\pi^+\pi^-\omega(\to \pi^+\pi^-\pi^0)$ contribution we assume about 0.07 μb taking $\mathcal{BR}(\omega \to \pi^+\pi^-\pi^0) = 0.89$ [47]. The narrow width of the η meson allows to impose an extra mass cut on the $\pi^+\pi^-\pi^0$ invariant mass and suppresses the multipion background efficiently. The reconstruction of this decay channel has a smaller efficiency ($\epsilon = 0.8\%$) compared to the $2\pi^+2\pi^-$ decay channel.

Figure 11(a) shows the reconstructed invariant mass of $\pi^+\pi^-\pi^0$ with a clear signal of η meson on top of a large background. The shape of this background was also studied by multipion production with uniform phase space distribution. No significant difference was found. A cut on the η meson mass $0.54\ \text{GeV} < M_{\pi^+\pi^-\pi^0} < 0.56$ GeV allows for efficient background subtraction and observation of $f_1(1285)$ meson peak [see Fig. 11(b)]. The expected signal (about 4000 counts) and background distributions in Fig. 11(b) display projections for about 30 days of measurement.

So far we have considered the 5-pion background with all components (1, 2, 3) listed in Table II. The contribution (1) can, in principle, be eliminated by using the side-band subtraction method. We wish to discuss now separately the contributions (2) and (4), in the $\pi^+\pi^-\eta$ mesonic state, to proof feasibility of the $f_1(1285)$ measurement. In Fig. 12 we make such a comparison. The nonreducible background contribution from double excitation of N^* resonances has a broader distribution than the $VV \to f_1$ signal. With our estimate of the cross section for the $pp \to ppf_1(1285)$ reaction (see Table II) we expect that the $f_1(1285)$ could be observed in the $\pi^+\pi^-\eta$ ($\to \pi^+\pi^-\pi^0$) channel.

Finally, the following comment on this measurement is in order. Since $f_1(1285)$ and $\eta(1295)$ are both decaying to the $\pi^+\pi^-\eta$ channel, care must be taken for potential overlap of these resonances with each other in the measurement. These two mesons are close in mass, but the $\eta(1295)$ has about 2 times larger total width than the $f_1(1285)$. Thus, precise mass measurements and/or partial-wave analyses

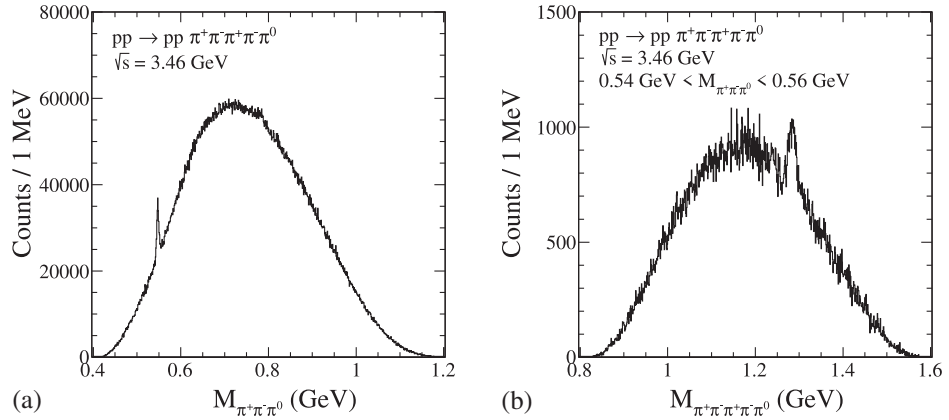

FIG. 11. Invariant mass distributions of (a) $\pi^+\pi^-\pi^0$ and (b) $\pi^+\pi^-\pi^+\pi^-\pi^0$ of the $pp\pi^+\pi^-\pi^+\pi^-\pi^0$ final state corresponding to the measurement with the $p+p$ reactions at $E_{\mathrm{kin}}=4.5$ GeV ($\sqrt{s}=3.46$ GeV) with the HADES apparatus. All components listed in Table II were included in the simulation. The result in panel (b) includes the cut on the η meson mass 0.54 GeV $< M_{\pi^+\pi^-\pi^0} <$ 0.56 GeV.

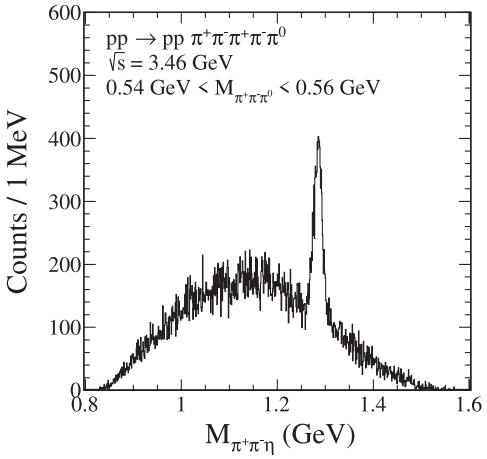

FIG. 12. Invariant mass distribution of $\pi^+\pi^-\eta$ observed in the $pp\pi^+\pi^-\pi^+\pi^-\pi^0$ final state corresponding to the measurement with the $p+p$ reactions at $E_{\mathrm{kin}}=4.5$ GeV ($\sqrt{s}=3.46$ GeV) with the HADES apparatus. Here, the two contributions (2) and (4) of Table II were included. The result includes the cut on the η meson mass 0.54 GeV $< M_{\pi^+\pi^-\pi^0} <$ 0.56 GeV.

must be done in order to distinguish both resonances. The distribution in the azimuthal angle ϕ_{pp} between the transverse momenta of the outgoing nucleons may also be used to disentangle f_1 and η contributions; see the discussion in Appendix E of [27]. There the following theorem was proven. If s-channel helicity conservation and helicity independence hold (as it is expected to be the case at high energies) the ϕ_{pp} distribution for CEP of η-type mesons must vanish for $\phi_{pp}=0$ and π. On the other hand, for the $f_1(1285)$ production via the VV-fusion mechanism we predict a strong preference for the outgoing nucleons to be produced with their transverse momenta being back-to-back ($\phi_{pp}\approx\pi$); see the right bottom panel of Fig. 7. But we have to ask if we can apply the above theorem to CEP of the $\eta(1295)$ in the threshold region. As for f_1 CEP we shall assume that the $\eta(1295)$ CEP near threshold occurs mainly through VV fusion ($V=\omega,\ \rho^0$) and that $g_{\omega\omega\eta(1295)}\sim g_{\rho\rho\eta(1295)}$. With the couplings of ρ and ω to protons from (2.13) we see that the helicity flipping tensor coupling of the ρ to the protons is large whereas the tensor coupling of the ω is small, actually taken to be zero in (2.13). Thus, near to the threshold the assumptions on which the above theorem rests are probably not well fulfilled. But at higher energies, available in the future at PANDA, $\omega\omega$ fusion giving $\eta(1295)$ should dominate over $\rho\rho$ fusion as is the case for f_1 production; see the right panels of Fig. 6. Then the ϕ_{pp} distribution for $\eta(1295)$ should (nearly) vanish for $\phi_{pp}=0$ and π. But clearly, if this becomes an important issue for the experiment, a complete calculation for CEP of the $\eta(1295)$ should be done along the same lines as done here for the f_1. For some estimates we note the following. In [17] the $g_{\eta(1295)\rho\gamma}$ coupling constant was estimated using the constituent quark model relationships for the two-photon width of the pseudoscalar mesons $\eta(1295)$, $\eta(1475)$ and the VMD model. The $g_{\eta(1295)\omega\gamma}$ coupling was estimated using the relation $g_{\eta(1295)\omega\gamma}=g_{\eta(1295)\rho\gamma}/3$ which is similar to the $f_1V\gamma$ coupling-constants relation (A3). The $\eta(1295)$ coupling constants found in [17] have small values and as a result the $\gamma p\to\eta(1295)p$ cross section was estimated to be smaller (about a factor 4) than the $\gamma p\to f_1(1285)p$ cross section. A greater difference between these cross sections, using the coupling constants from [17], was found in [21]. The results on photoproduction indicate that also CEP of the $\eta(1295)$ in proton-(anti)proton collisions should be smaller than the $f_1(1285)$ production. This suggests that the measurements of the $f_1(1285)$ should be possible, even without a detailed partial wave analysis, in the HADES / PANDA kinematics.

V. CONCLUSIONS

In the present paper we have discussed the possibility to observe the $f_1(1285)$ in the $pp\to ppf_1(1285)$ reaction at

energies close to the threshold where the Pomeron-Pomeron fusion, known to be the dominant mechanism at high energies, is expected to give only a very small contribution. Two different mechanisms have been considered: (a) $\omega\omega \to f_1(1285)$ fusion and (b) $\rho^0\rho^0 \to f_1(1285)$ fusion. We have estimated the cross section for $\sqrt{s} = 3.46$ GeV for which a measurement will soon be possible for HADES@GSI.

We have presented our method for the derivation of the $VV \to f_1(1285)$ vertex for $V = \rho^0, \omega$. The coupling constant $g_{\rho\rho f_1}$ has been extracted from the decay rate of $f_1 \to \rho^0\gamma$ using the VMD ansatz. From naive quark model and VMD relations we have obtained equality of the $g_{\rho\rho f_1}$ and the $g_{\omega\omega f_1}$ coupling constants; see Appendix A. In reality this relation can be expected to hold at the 20% level. Then, we have fixed the cutoff parameters in the form factors and the corresponding coupling constants by fits to the CLAS experimental data for the process $\gamma p \to f_1(1285)p$. There, the ρ- and ω-exchange contributions play a crucial role in reproducing the forward-peaked angular distributions, especially at higher energies, $W_{\gamma p} > 2.55$ GeV.

The corresponding $\rho\rho$ and $\omega\omega$ fusion amplitudes have been written out explicitly. The two amplitudes have been used to estimate the total and differential cross sections for c.m. energy $\sqrt{s} = 3.46$ GeV. The energy dependence close to the threshold has been discussed. The distributions in t (see Fig. 6) and the distributions in $\cos\theta_M$ (see Fig. 9) seem particularly interesting. The shape of these distributions gives information on the role of the individual fusion processes.

We have discussed the possibility of a measurement of the $pp \to ppf_1(1285)$ reaction by the HADES collaboration at GSI. For this, the $\pi^+\pi^-\pi^+\pi^-$, $\rho^0\gamma$, and $\pi^+\pi^-\eta$ channels, have been considered. For the four-pion channel we have estimated the background using the cross section from an old bubble chamber experiment [53]. We have found that the double excitation of the $N(1440)$ resonances via the σ-meson exchange is probably the dominant mechanism in the $pp \to pp2\pi^+2\pi^-$ reaction. The mechanisms considered by us: $\pi^0 - \omega - \pi^0$ and $\omega - \pi^0 - \omega$ exchanges give much smaller background cross sections. We conclude that it may be difficult to identify the $f_1(1285)$ meson in this channel. The $\rho^0\gamma$ channel should be much better suited as far as signal-to-background ratio is considered. There, however, the dominant background channel $pp\pi^+\pi^-\pi^0$ is of the order of 2 mb [53] and the ρ^0 is so broad that cuts on its mass will not provide sufficient background reductions. This is very different for the decay channel $f_1 \to \pi^+\pi^-\eta(\to \pi^+\pi^-\pi^0)$ since the η has a very small width and a cut on the η mass will reduce the background efficiently. We have performed feasibility studies and estimated that a 30-days measurement with HADES should allow to identify the $f_1(1285)$ meson in the $pp\pi^+\pi^-\eta$ final state. No simulation of the $\pi^+\pi^-\eta(\to \pi^+\pi^-\pi^0)$ channel has been done for PANDA energies.

In [71] the $f_1(1285)$ decays into $a_0(980)\pi^0$, $f_0(980)\pi^0$ and isospin breaking were studied. An interesting proposal was also discussed in [72,73]: to study the anomalous isospin breaking decay $f_1(1285) \to \pi^+\pi^-\pi^0$ in central exclusive production of the f_1. There is another important decay channel, $K\bar{K}\pi$, with branching fraction 9% [47] which can be used for f_1 meson studies in CEP. See also [74] for a discussion of the $K\bar{K}\pi$ decay and the nature of the $f_1(1285)$ meson.

Predictions for the PANDA experiment at FAIR, for the $p\bar{p} \to p\bar{p}f_1(1285)$ reaction, have also been presented. The possibility to study the underlying reaction mechanisms have been discussed. For the $VV \to f_1(1285)$ fusion processes for $\sqrt{s} = 5.0$ GeV we have obtained about 10 times larger cross sections than for $\sqrt{s} = 3.46$ GeV. Thus we predict a large cross section for the exclusive axial-vector $f_1(1285)$ production for the PANDA energy range.

To conclude: we have shown that the study of $f_1(1285)$ production at HADES and PANDA should be feasible. From such experiments we will learn more on the nature of the f_1. For instance, is it a normal $q\bar{q}$ state or $\bar{K}K^*$ molecule [74,75]? Can it be described in holographic QCD [18]? In particular, we shall learn from f_1 CEP at low energies about the $\rho\rho f_1$ and $\omega\omega f_1$ coupling strengths. These in turn are very interesting parameters for the calculations of light-by-light contributions to the anomalous magnetic moment of the muon [10–15]. The final aim for studies of f_1 CEP in proton-proton collisions should be to have a good understanding of this reaction, both from theory and from experiment, in the near threshold region, in the intermediate energy region 8 GeV $\lesssim \sqrt{s} \lesssim$ 30 GeV, and up to high energies available at the LHC as discussed in [27].

ACKNOWLEDGMENTS

We are indebted to Kanzo Nakayama for a discussion of FSI effect in the $pp \to ppM$ reactions and Johann Haidenbauer for exchange of information on excitations of nucleon resonances. This work was partially supported by the Polish National Science Centre under Grant No. 2018/31/B/ST2/03537 and by the Center for Innovation and Transfer of Natural Sciences and Engineering Knowledge in Rzeszów (Poland).

APPENDIX A: ON THE RELATION OF $g_{\rho\rho f_1}$ AND $g_{\omega\omega f_1}$

Here we discuss some simple theoretical ideas on the relation of these two coupling parameters. First we note that isospin symmetry alone provides *no* relation. We shall use the most naive quark model and VMD to get a handle on the ratio $g_{\rho\rho f_1}/g_{\omega\omega f_1}$.

In the simple naive quark model the f_1, ρ^0 and ω mesons are represented with the following quark content

$$f_1(1285) \sim \frac{1}{\sqrt{2}}(u\bar{u} + d\bar{d}),$$
$$\rho^0 \sim \frac{1}{\sqrt{2}}(u\bar{u} - d\bar{d}),$$
$$\omega \sim \frac{1}{\sqrt{2}}(u\bar{u} + d\bar{d}). \tag{A1}$$

Consider now a radiative decay of the f_1. After the emission of the photon by the f_1 the quark state should have the structure, with the quark charges $e_u = 2/3$, $e_d = -1/3$, $e_s = -1/3$:

$$\begin{aligned}\gamma f_1 &\sim \frac{1}{\sqrt{2}}(e_u u\bar{u} + e_d d\bar{d}) \\ &= \frac{1}{2}(e_u + e_d)\frac{1}{\sqrt{2}}(u\bar{u} + d\bar{d}) + \frac{1}{2}(e_u - e_d)\frac{1}{\sqrt{2}}(u\bar{u} - d\bar{d}) \\ &\sim \frac{1}{6}\omega + \frac{1}{2}\rho^0. \end{aligned} \tag{A2}$$

Therefore, this simple argument suggests for the $f_1 V\gamma$ coupling constants the relation

$$\frac{g_{f_1\rho\gamma}}{g_{f_1\omega\gamma}} = 3. \tag{A3}$$

This is the relation suggested, e.g., in [17].

Now we can combine this with VMD which allows to relate the g_{VVf_1} and $g_{f_1V\gamma}$ by the standard $V\gamma$ transition vertices; see e.g., (3.23)–(3.25) of [28]. This gives, with $e = \sqrt{4\pi\alpha_{\rm em}}$,

$$g_{f_1V\gamma} = \frac{e}{\gamma_V} g_{VVf_1}, \tag{A4}$$

where $\gamma_\rho > 0$, $\gamma_\omega > 0$, and

$$\frac{4\pi}{\gamma_\rho^2} = 0.496 \pm 0.023, \qquad \frac{4\pi}{\gamma_\omega^2} = 0.042 \pm 0.0015. \tag{A5}$$

In the naive quark model plus VMD the hadronic light-quark-electromagnetic current is written as follows:

$$\begin{aligned} J_\mu^{\rm em} &= e[e_u \bar{u}\gamma_\mu u + e_d \bar{d}\gamma_\mu d + e_s \bar{s}\gamma_\mu s] \\ &= e\left\{\frac{1}{\sqrt{2}}(e_u - e_d)\frac{1}{\sqrt{2}}(\bar{u}\gamma_\mu u - \bar{d}\gamma_\mu d)\right. \\ &\quad \left. + \frac{1}{\sqrt{2}}(e_u + e_d)\frac{1}{\sqrt{2}}(\bar{u}\gamma_\mu u + \bar{d}\gamma_\mu d) + e_s \bar{s}\gamma_\mu s\right\} \\ &= e\left\{\frac{m_\rho^2}{\gamma_\rho^{(\rm id)}}\rho_\mu^{(0)} + \frac{m_\omega^2}{\gamma_\omega^{(\rm id)}}\omega_\mu + \frac{m_\phi^2}{\gamma_\phi^{(\rm id)}}\phi_\mu\right\}. \end{aligned} \tag{A6}$$

Assuming $m_\rho^2 = m_\omega^2$ (which is quite good) and $m_\rho^2 = m_\phi^2$ (which is less good) we find from (A6) the following "ideal mixing" coupling ratios:

$$\frac{\gamma_\omega^{(\rm id)}}{\gamma_\rho^{(\rm id)}} = \frac{e_u - e_d}{e_u + e_d} = 3, \qquad \frac{\gamma_\phi^{(\rm id)}}{\gamma_\rho^{(\rm id)}} = \frac{e_u - e_d}{\sqrt{2}e_s} = -\frac{3}{\sqrt{2}}. \tag{A7}$$

From (A4) and (A7) we obtain with the "ideal" γV couplings

$$\frac{g_{f_1\rho\gamma}}{g_{f_1\omega\gamma}} = \frac{\gamma_\omega^{(\rm id)}}{\gamma_\rho^{(\rm id)}}\frac{g_{\rho\rho f_1}}{g_{\omega\omega f_1}} = 3\frac{g_{\rho\rho f_1}}{g_{\omega\omega f_1}}. \tag{A8}$$

With (A3) plus (A8) we obtain, thus, the simple estimate

$$\frac{g_{\rho\rho f_1}}{g_{\omega\omega f_1}} = 1, \tag{A9}$$

based on naive quark-model relations plus the simplest VMD ansatz.

If we include form factors in our considerations as in (2.8)–(2.11) we will get instead of (A4)

$$g_{f_1V\gamma} = \frac{e}{\gamma_V} g_{VVf_1}\tilde{F}_V(0); \tag{A10}$$

see also Appendix B below. Assuming $\tilde{F}_\rho(0) = \tilde{F}_\omega(0)$ we get again the relation (A9).

In reality we get from (A5), using the central values there,

$$\frac{\gamma_\omega}{\gamma_\rho} = 3.44. \tag{A11}$$

That is, ideal mixing (A7) gives only an approximation, valid to within 15%, compared to the experimental value (A11). We can, therefore, expect that also the relation (A9) may be violated in the real world by 15 to 20%.

We emphasize that the arguments presented in this Appendix depend crucially on the assumption made in (A1) that the $f_1(1285)$ is a normal $q\bar{q}$ state. The relation (A3) in particular could be quite different if this assumption is violated and the $f_1(1285)$ has another structure. In [74,75], for instance, the $f_1(1285)$ is described as a $K^*\bar{K}$ molecule, not as a $q\bar{q}$ state.

APPENDIX B: THE RADIATIVE DECAYS OF THE $f_1(1285)$ MESON AND THE $\rho\rho f_1$ COUPLING CONSTANT

In this Appendix we shall discuss the radiative decays of the $f_1(1285)$ meson using VMD and the VVf_1 coupling vertex (2.8) for $V = \rho^0$. We consider two theoretical treatments. In the first method we consider the decay $f_1 \to \rho^0\gamma$ with a fixed mass for the ρ^0 meson:

$$f_1(k, \epsilon^{(f_1)}) \to \rho^0(k_\rho, \epsilon^{(\rho)}) + \gamma(k_\gamma, \epsilon^{(\gamma)}). \tag{B1}$$

In the second method we consider the decay $f_1 \to \pi^+\pi^-\gamma$ via an intermediate ρ^0 meson taking its mass distribution into account:

$$f_1(k,\epsilon^{(f_1)}) \to [\rho^0(k_\rho) \to \pi^+(k_1) + \pi^-(k_2)] + \gamma(k_\gamma,\epsilon^{(\gamma)}). \tag{B2}$$

From (B1) and (B2) we will estimate the $g_{\rho\rho f_1}$ coupling constant and the cutoff parameter Λ_V in the form factor $F_{\rho\rho f_1}$ from experiment.

The amplitude for the reaction (B1) is given by

$$\begin{aligned}\mathcal{M}_{\lambda_{f_1}\to\lambda_\rho\lambda_\gamma} &= (-i)(\epsilon^{(\rho)\mu}(\lambda_\rho))^*(\epsilon^{(\gamma)\nu}(\lambda_\gamma))^* i\Gamma^{(\rho\rho f_1)}_{\mu\nu''\alpha}(-k_\rho,-k_\gamma)\\ &\times i\Delta^{(\rho)\nu''\nu'}(k_\gamma) i\Gamma^{(\rho\to\gamma)}_{\nu'\nu}(k_\gamma)\epsilon^{(f_1)\alpha}(\lambda_{f_1})\\ &= \frac{e}{\gamma_\rho}(\epsilon^{(\rho)\mu}(\lambda_\rho))^*(\epsilon^{(\gamma)\nu}(\lambda_\gamma))^*\Gamma^{(\rho\rho f_1)}_{\mu\nu\alpha}\\ &\times(-k_\rho,-k_\gamma)\epsilon^{(f_1)\alpha}(\lambda_{f_1}),\end{aligned} \tag{B3}$$

where $\epsilon^{(\rho)}$, $\epsilon^{(\gamma)}$ and $\epsilon^{(f_1)}$ are the polarization vectors for ρ^0, photon and $f_1(1285)$ meson with the four-momenta and helicities k_ρ, $\lambda_\rho = \pm1, 0$, k_γ, $\lambda_\gamma = \pm1$ and k, $\lambda_{f_1} = \pm1, 0$, respectively. We use the VMD ansatz for the coupling of the ρ^0 meson to the photon; see e.g., (3.23)–(3.25) of [28]. We assume in the $\Gamma^{(\rho\rho f_1)}$ vertex (2.8) the form factor according to (2.10)

$$\begin{aligned}F_{\rho\rho f_1}(k_\rho^2,k_\gamma^2,k^2) &= F_{\rho\rho f_1}(m_\rho^2,0,m_{f_1}^2)\\ &= \tilde{F}_\rho(m_\rho^2)\tilde{F}_\rho(0)F_{f_1}(m_{f_1}^2) = \tilde{F}_\rho(0),\end{aligned} \tag{B4}$$

with $\tilde{F}_\rho(0)$ given in (2.11).

The amplitude for the reaction (B2), $\mathcal{M}_{\lambda_{f_1}\to\pi^+\pi^-\lambda_\gamma}$, is obtained from (B3) by making the replacement

$$\begin{aligned}(\epsilon^{(\rho)\mu}(\lambda_\rho))^* &\to i\Delta^{(\rho)\mu\mu'}(k_\rho) i\Gamma^{(\rho\pi\pi)}_{\mu'}(k_1,k_2)\\ &= -\frac{g_{\rho\pi\pi}}{2}(k_1-k_2)^\mu\Delta_T^{(\rho)}(k_\rho^2),\end{aligned} \tag{B5}$$

and taking

$$F_{\rho\rho f_1}(k_\rho^2,k_\gamma^2,k^2) = F_{\rho\rho f_1}(k_\rho^2,0,m_{f_1}^2) = \tilde{F}_\rho(k_\rho^2)\tilde{F}_\rho(0) \tag{B6}$$

with $k_\rho^2 = (k_1+k_2)^2$. The ρ^0 propagator function and the $\rho^0\pi^+\pi^-$ coupling in (B5) are taken from (4.1)–(4.6) and (3.35), (3.36) of [28], respectively.

Then, the coupling constant $g_{\rho\rho f_1}$, occurring in $\Gamma^{(\rho\rho f_1)}$ in the amplitudes above, can be adjusted to the experimental decay width $\Gamma(f_1(1285)\to\gamma\rho^0)$. For the $1\to2$ decay process (B1) this is straightforward. For the $1\to3$ decay process (B2) this will be done with the help of a new Monte Carlo generator DECAY [76] designed for a general decay of the $1\to n$ type.

Unfortunately the partial decay width $\Gamma(f_1(1285)\to\gamma\rho^0)$ appears to be not well known in the literature, see also the discussion in Sec. VII C and Table IV in [16],

$$\text{from PDG [47]: } \Gamma(f_1(1285)\to\gamma\rho^0) = 1384.7^{+305.1}_{-283.1}\ \text{keV}, \tag{B7}$$

$$\text{from CLAS [16]: } \Gamma(f_1(1285)\to\gamma\rho^0) = (453\pm177)\ \text{keV}. \tag{B8}$$

Using the values of total widths accordingly from PDG (2.27) and the CLAS experiment (2.28) we get

$$\text{from PDG [47]: } \mathcal{BR}(f_1(1285)\to\gamma\rho^0) = (6.1\pm1.0)\%, \tag{B9}$$

$$\text{from CLAS [16]: } \mathcal{BR}(f_1(1285)\to\gamma\rho^0) = (2.5^{+0.7}_{-0.8})\%. \tag{B10}$$

We note that the CLAS result is in agreement with that found in [77],

$$\mathcal{BR}(f_1(1285)\to\gamma\rho^0) = (2.8\pm0.7(\text{stat})\pm0.6(\text{syst}))\%, \tag{B11}$$

where the decay $f_1(1285)\to\rho^0\gamma$ was studied in the reaction $\pi^-N\to\pi^-f_1N$. Theoretical estimates based on the QCD inspired models such as the covariant oscillator quark model [78] and the Nambu–Jona-Lasinio model [8], which assume that the $f_1(1285)$ has a quark-antiquark nature, suggest (B8) rather than (B7). We hope that the future experimental measurements can clarify this issue. In the following we shall use both values, (B7) and (B8), to highlight the problem.

In Table III we collect our results for the two processes (B1) and (B2) obtained from (B7) and (B8). In the calculations we take $m_\rho = 775$ MeV. We show results for the cutoff parameter from $\Lambda_\rho = 0.65$ GeV to 2 GeV in (2.11). We expect the upper limit of the $\rho\rho f_1$ coupling constant to be not much larger than $|g_{\rho\rho f_1}| \simeq 20$. Otherwise one gets a nonrealistically large cutoff parameter Λ_{VNN} in the VNN vertex (see the discussion in Appendix C).

It is also interesting to compare our results with those of [75]. In [75] the radiative decays $f_1(1285)\to\gamma V$ were evaluated with the assumption that the $f_1(1285)$ is dynamically generated from the $K^*\bar{K}$ interaction. In this model the partial decay widths strongly depend on the cutoff parameter Λ, for instance, $\Gamma(f_1(1285)\to\gamma\rho^0) = 420$ keV, or 880 keV, for $\Lambda = 0.8$ GeV, or 1.5 GeV, respectively; see Table I of [75]. Moreover, there were also determined the ratios

$$R_1 = \frac{\Gamma(f_1\to\gamma\rho^0)}{\Gamma(f_1\to\gamma\phi)} \simeq 60, \tag{B12}$$

TABLE III. Coupling constant $|g_{\rho\rho f_1}|$ extracted from our model analysis of the radiative decays of the $f_1(1285)$. The results correspond to the two central values of $\Gamma(f_1(1285) \to \gamma\rho^0)$ from (B7) ("PDG") and (B8) ("CLAS"), respectively, and to various values of the cutoff parameter Λ_ρ in (2.11).

Process	Cutoff parameter	PDG, $\lvert g_{\rho\rho f_1}\rvert$	CLAS, $\lvert g_{\rho\rho f_1}\rvert$
$f_1 \to \rho^0\gamma$, Eq. (B1)	$\Lambda_\rho = 0.65$ GeV	27.37	15.66
	$\Lambda_\rho = 0.7$ GeV	22.68	12.97
	$\Lambda_\rho = 1.0$ GeV	12.33	7.05
	$\Lambda_\rho = 2.0$ GeV	9.27	5.30
$f_1 \to \pi^+\pi^-\gamma$, Eq. (B2)	$\Lambda_\rho = 0.65$ GeV	35.02	20.03
	$\Lambda_\rho = 0.7$ GeV	28.54	16.33
	$\Lambda_\rho = 0.8$ GeV	20.98	12.00
	$\Lambda_\rho = 0.9$ GeV	17.05	9.75
	$\Lambda_\rho = 1.0$ GeV	14.85	8.49
	$\Lambda_\rho = 1.5$ GeV	11.52	6.59
	$\Lambda_\rho = 2.0$ GeV	10.97	6.27

$$R_2 = \frac{\Gamma(f_1 \to \gamma\rho^0)}{\Gamma(f_1 \to \gamma\omega)} \simeq 30. \tag{B13}$$

The dependence of both ratios on the cutoff parameter is rather weak. In the model of [75] the partial decay width of $\Gamma(f_1 \to \gamma\rho^0)$ is much larger than the ones of the $\gamma\omega$ and $\gamma\phi$ channels due to constructive (destructive) interference of the triangle loop diagrams for the ρ^0 (ω and ϕ) production.

Now we consider the decay $f_1 \to \omega\gamma$ in our approach. We use the formula of (B3) with the replacements $\rho \to \omega$ [$\gamma_\rho \to \gamma_\omega$ (A5), $g_{f_1\rho\rho} \to g_{f_1\omega\omega}$, $m_\rho \to m_\omega$]. In the calculation we take $m_\omega = 783$ MeV. We assume $g_{\omega\omega f_1} = g_{\rho\rho f_1}$ (A9) and take $g_{\rho\rho f_1}$ corresponding to $\Lambda_\rho = 0.65$ GeV and 2.0 GeV from Table III ($f_1 \to \rho^0\gamma$).

With $\Lambda_\rho = 0.65$ GeV (first line in Table III), we obtain $\Gamma(f_1 \to \gamma\omega) = 106.61$ keV for $|g_{f_1\omega\omega}| = 27.37$ and $\Gamma(f_1 \to \gamma\omega) = 34.90$ keV for $|g_{f_1\omega\omega}| = 15.66$. Using the central values of (B7) and (B8) these correspond to the ratios of $R_2 = 12.98$ and $R_2 = 12.99$, respectively. With $\Lambda_\rho = 2.0$ GeV (fourth line in Table III), we obtain $\Gamma(f_1 \to \gamma\omega) = 112.61$ keV for $|g_{f_1\omega\omega}| = 9.27$ and $\Gamma(f_1 \to \gamma\omega) = 36.81$ keV for $|g_{f_1\omega\omega}| = 5.30$. With the central values of (B7) and (B8) we obtain the ratios $R_2 = 12.31$ and $R_2 = 12.30$, respectively. These values for R_2 are similar to the result in [78] (see set b for the mixing angle $\phi_A = 21°$ of Table XI therein) but are about 2 times smaller than (B13) estimated in [75].

The recent average for R_1 given by PDG [47] is $R_1 = 82.4^{+11.4}_{-23.8}$. This is about 1 s.d. away from the theoretical result (B12) of [75]. But we have to keep in mind the differences in the width of $f_1 \to \gamma\rho^0$ given by PDG and CLAS; see (B7) and (B8). There are currently no experimental data available for $f_1(1285) \to \gamma\omega$ decay. Further experiments will hopefully clarify the situation.

APPENDIX C: PHOTOPRODUCTION OF THE $f_1(1285)$ MESON AND COMPARISON WITH THE CLAS EXPERIMENTAL DATA

Here we discuss the photoproduction of the $f_1(1285)$ meson. Using VMD and the g_{VVf_1} coupling constants introduced in (2.8) we have to calculate the diagram shown in Fig. 13. The differential cross section for the reaction $\gamma p \to f_1(1285)p$ will be compared with the CLAS data [16]. From this we will estimate the form factor and cutoff parameters of the model.

The unpolarized differential cross section for the reaction $\gamma p \to f_1(1285)p$ is given by

$$\frac{d\sigma}{d\Omega} = \frac{1}{64\pi^2 s}\frac{|k|}{|q|}\frac{1}{4}\sum_{\text{spins}}|\mathcal{M}_{\gamma p \to f_1(1285)p}|^2,$$
$$d\Omega = \sin\theta d\theta d\phi. \tag{C1}$$

Here we work in the center-of-mass (c.m.) frame, s is the invariant mass squared of the γp system, and q and k are the c.m. three-momenta of the initial photon and final $f_1(1285)$, respectively. Taking the direction of q as a z axis we denote the polar and azimuthal angles of k by θ and ϕ.

We use standard kinematic variables

$$s = W_{\gamma p}^2 = (p_b + q)^2 = (p_2 + k)^2,$$
$$q_t = p_b - p_2 = k - q, \qquad t = q_t^2. \tag{C2}$$

The amplitude for the $\gamma p \to f_1(1284)p$ reaction via the vector-meson exchange includes two terms

$$\mathcal{M}_{\gamma p \to f_1(1285)p} = \mathcal{M}^{(\rho\,\text{exchange})} + \mathcal{M}^{(\omega\,\text{exchange})}. \tag{C3}$$

The generic amplitude with $V = \rho^0, \omega$, for the diagram in Fig. 13, can be written as

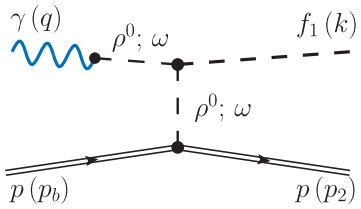

FIG. 13. Photoproduction of an f_1 meson via vector-meson exchanges.

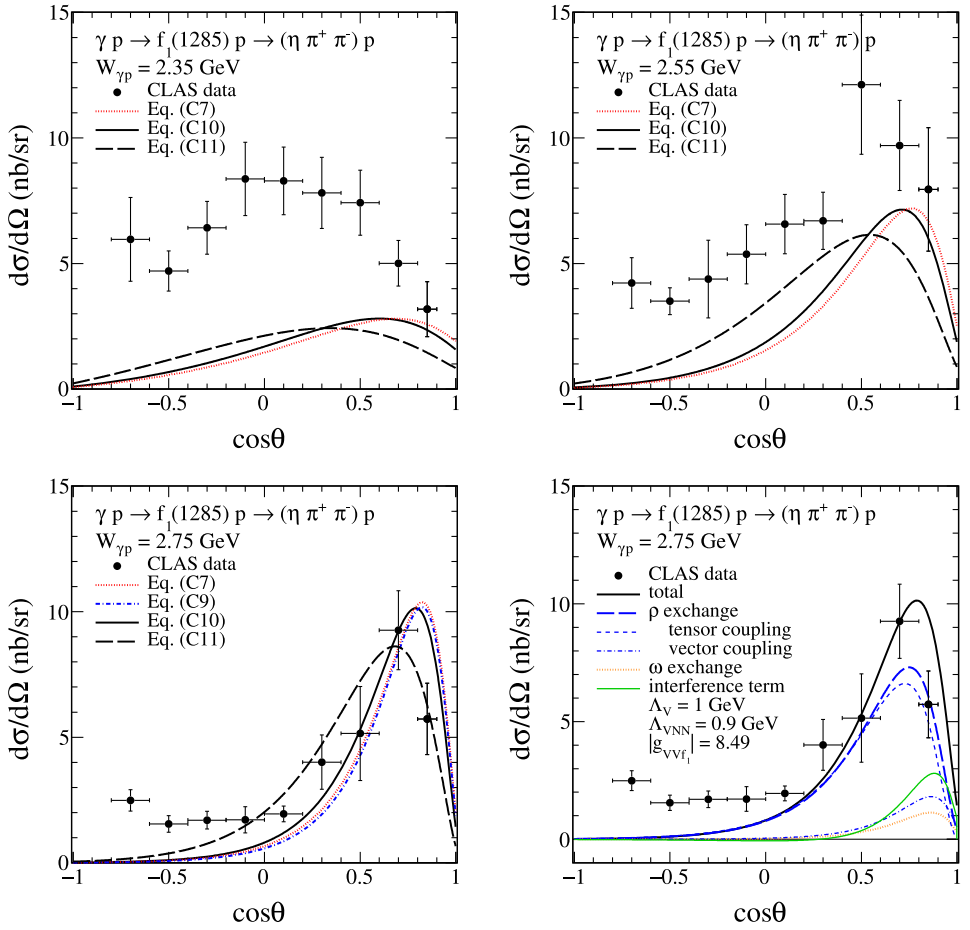

FIG. 14. The differential cross sections for the reaction $\gamma p \to f_1(1285)p \to \eta\pi^+\pi^- p$. Data are taken from Table V of [16]. The vertical error bars are the statistical and systematic uncertainties. Our results are scaled by a factor of 0.35 to account for the branching fraction from $f_1(1285) \to \eta\pi^+\pi^-$ (C6). We take the Vpp coupling constants from (2.13) and the different values of g_{VVf_1} corresponding to Λ_V from the column "CLAS" of Table III. In the bottom right panel we show the individual contributions of ρ and ω exchanges and their coherent sum (total) at $W_{\gamma p} = 2.75$ GeV. For the ρ-exchange contribution also the results for only one type of coupling, tensor or vector, in the ρ-proton vertex (2.12) are shown.

$$\langle f_1(k,\lambda_{f_1}), p(p_2,\lambda_2)|\mathcal{T}|\gamma(q,\lambda_\gamma), p(p_b,\lambda_b)\rangle \equiv \mathcal{M}^{(V\text{exchange})}_{\lambda_\gamma\lambda_b\to\lambda_{f_1}\lambda_2} = (-i)(\epsilon^{(f_1)\alpha}(\lambda_{f_1}))^* i\Gamma^{(VVf_1)}_{\mu''\nu'\alpha}(q,q_t) i\Delta^{(V)\mu''\mu'}(q) i\Gamma^{(\gamma\to V)}_{\mu'\mu}(q)\epsilon^{(\gamma)\mu}(\lambda_\gamma) \times i\tilde{\Delta}^{(V)\nu'\nu}(s,t)\bar{u}(p_2,\lambda_2) i\Gamma^{(Vpp)}_{\nu}(p_2,p_b)u(p_b,\lambda_b), \tag{C4}$$

where p_b, p_2 and λ_b, $\lambda_2 = \pm\frac{1}{2}$ denote the four-momenta and helicities of the incoming and outgoing protons.

We use the relations for the $\gamma - V$ couplings ($V = \rho^0, \omega$) from (A4) and (A5). For the other building blocks of the amplitude (C4) see (2.8)–(2.21) in Sec. II. We can then write

$$\mathcal{M}^{(V\text{exchange})}_{\lambda_\gamma\lambda_b\to\lambda_{f_1}\lambda_2} = -\frac{e}{\gamma_V}(\epsilon^{(f_1)\alpha}(\lambda_{f_1}))^* i\Gamma^{(VVf_1)}_{\mu\nu\alpha}(q,q_t)\epsilon^{(\gamma)\mu}(\lambda_\gamma)\tilde{\Delta}^{(V)}_T(s,t)\bar{u}(p_2,\lambda_2) i\Gamma^{(Vpp)\nu}(p_2,p_b)u(p_b,\lambda_b). \tag{C5}$$

We perform the calculation of the total and differential cross sections with the cutoff parameter Λ_ρ and corresponding VVf_1 coupling constant g_{VVf_1} from Table III. We choose the values from the last column (CLAS). For instance, $|g_{\rho\rho f_1}| = 8.49$ corresponds to $\Lambda_\rho = 1.0$ GeV and $|g_{\rho\rho f_1}| = 20.03$ corresponds to $\Lambda_\rho = 0.65$ GeV. We assume $g_{\omega\omega f_1} = g_{\rho\rho f_1} \equiv g_{VVf_1}$; see (A9). For the Vpp coupling constants we take (2.13). For the V-proton form factor $F_{VNN}(t)$ we take the monopole form as in (2.15) with the parameter Λ_{VNN} to be extracted from the CLAS data.

In Fig. 14 we compare our results for the photoproduction of $f_1(1285)$ meson with the CLAS data [16]. Since the

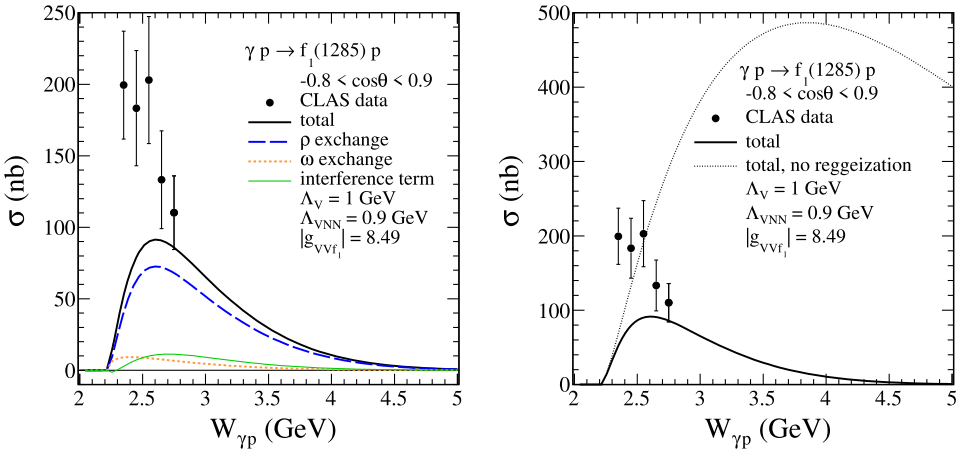

FIG. 15. The elastic $f_1(1285)$ photoproduction cross section as a function of the center-of-mass energy $W_{\gamma p}$. Five data points are obtained by integrating out the differential cross sections given in Table V of [16]. The experimental results have been scaled by the branching fraction $\mathcal{BR}(f_1(1285) \to \eta\pi^+\pi^-) = 0.35$; see (C6). We take the coupling parameters the same as in the bottom right panel of Fig. 14. We integrate for $-0.8 < \cos\theta < 0.9$. In the left panel the Reggeized contributions of ρ and ω exchanges, their coherent sum (total), and the interference term are shown. In the right panel the solid line is the result from the Reggeized model, the dotted line indicates the result without the Reggeization.

CLAS Collaboration presents the differential cross sections for $\gamma p \to f_1(1285)p \to \eta\pi^+\pi^- p$, our theoretical curves in Fig. 14 have been scaled by the branching fraction $\mathcal{BR}(f_1(1285) \to \eta\pi^+\pi^-) = 0.35$ from [47]

$$\mathcal{BR}(f_1(1285) \to \eta\pi^+\pi^-) = 0.35 \pm 0.15. \quad \text{(C6)}$$

From Fig. 14 we see that with the Reggeized ρ and ω exchanges we describe the CLAS experimental data [16] at $W_{\gamma p} = 2.75$ GeV in the forward scattering region. $d\sigma/d\cos\theta$ decreases rapidly at forward angles, $\cos\theta = 1$. We cannot expect our exchange model to also describe the data at the lower CLAS energies since there we must expect s-channel resonances and u-channel nucleon exchanges to become important; see e.g., [20]. The model results are very sensitive on the form-factor cutoff parameters Λ_V and Λ_{VNN} at the VVf_1 and VNN vertices ($V = \rho,\ \omega$). Fitting the CLAS experimental data at $W_{\gamma p} = 2.75$ GeV we find

$$\Lambda_{VNN} = 1.35\,\text{GeV} \ \text{ for } \Lambda_V = 0.65\,\text{GeV}, \quad |g_{VVf_1}| = 20.03; \quad \text{(C7)}$$

$$\Lambda_{VNN} = 1.17\,\text{GeV} \ \text{ for } \Lambda_V = 0.7\,\text{GeV}, \quad |g_{VVf_1}| = 16.33; \quad \text{(C8)}$$

$$\Lambda_{VNN} = 1.01\,\text{GeV} \ \text{ for } \Lambda_V = 0.8\,\text{GeV}, \quad |g_{VVf_1}| = 12.0; \quad \text{(C9)}$$

$$\Lambda_{VNN} = 0.9\,\text{GeV} \ \text{ for } \Lambda_V = 1.0\,\text{GeV}, \quad |g_{VVf_1}| = 8.49; \quad \text{(C10)}$$

$$\Lambda_{VNN} = 0.834\,\text{GeV} \ \text{ for } \Lambda_V = 1.5\,\text{GeV}, \quad |g_{VVf_1}| = 6.59; \quad \text{(C11)}$$

$$\Lambda_{VNN} = 0.82\,\text{GeV} \ \text{ for } \Lambda_V = 2.0\,\text{GeV}, \quad |g_{VVf_1}| = 6.27. \quad \text{(C12)}$$

There is not much difference between the angular distributions resulting from the four parameter sets (C7)–(C10). The results for $\Lambda_{VNN} < 0.9$ GeV in the monopole form factor (2.15) are rather unrealistic, Λ_{VNN} being too close to the vector meson masses m_ρ, m_ω. Note that the value of $\Lambda_{VNN} = 1.35$ GeV is close to the values used in the Bonn potential model: $\Lambda_{\rho NN} = 1.4$ GeV and $\Lambda_{\omega NN} = 1.5$ GeV; see Table IV of [32]. Therefore, we are left with the sets of parameters (C7)–(C10) for our considerations in the $pp \to ppf_1$ reaction.

In the bottom right panel of Fig. 14 the individual ρ- and ω-exchange contributions at $W_{\gamma p} = 2.75$ GeV are shown. Here we use the parameters given in (C10). The ρ-exchange term is larger than the ω-exchange term due to larger coupling constants both in the $\gamma \to V$ transition vertex (A5), (A11) and for the tensor coupling in the V-proton vertex (2.12), (2.13). The differential distribution at $W_{\gamma p} = 2.75$ GeV peaks for $\cos\theta = 0.7$ corresponding to $-t = 0.66\ \text{GeV}^2$. The tensor coupling in the ρ-proton vertex with parameters $\kappa_\rho F_{\rho NN}(t)$ plays the most important role there. One can observe also an interference effect between the ρ and ω exchange terms.[3]

[3]In [21] a different relation for the coupling constants was used, namely $g_{f_1\omega\gamma} = -g_{f_1\rho\gamma}/3$ instead of (A3). The relative sign of these couplings has physical significance in the process $\gamma p \to f_1(1285)p$ as the ρ- and ω-exchange terms interfere. Therefore, the corresponding cross sections, see Figs. 5 and 6 of [21], are different from ours.

In Fig. 15 we show the integrated cross sections for the reaction $\gamma p \to f_1(1285)p$ together with the CLAS data. Results for $-0.8 < \cos\theta < 0.9$ are presented. In the calculation we take (C10). In the left panel we show the respective contributions of ρ and ω exchanges and their coherent sum with the same V-proton coupling parameters as in the bottom right panel of Fig. 14. There, for $W_{\gamma p} \simeq 2.7$ GeV, a large interference between the ρ exchange term and the ω exchange term can be observed. In the right panel we compare our Reggeized model results with those of the model without this effect. We note that the form of Reggeization used in our model, calculated according to (2.17)–(2.21), affects both, the t-dependence of the V exchanges, and the size of the cross section.

[1] G. Gidal *et al.*, Observation of Spin-1 $f_1(1285)$ in the Reaction $\gamma\gamma^* \to \eta^0\pi^+\pi^-$, Phys. Rev. Lett. **59**, 2012 (1987).

[2] H. Aihara *et al.*, (TPC/Two-Gamma Collaboration), $f_1(1285)$ formation in photon-photon fusion reactions, Phys. Lett. B **209**, 107 (1988).

[3] H. Aihara *et al.*, (TPC/Two-Gamma Collaboration), Formation of spin-one mesons by photon-photon fusion, Phys. Rev. D **38**, 1 (1988).

[4] P. Achard *et al.* (L3 Collaboration), $f_1(1285)$ formation in two-photon collisions at LEP, Phys. Lett. B **526**, 269 (2002).

[5] F. E. Close, Filtering glueball from $q\bar{q}$ production in proton proton or double tagged $e^+e^- \to e^+e^-R$ and implications for the spin structure of the Pomeron, Phys. Lett. B **419**, 387 (1998).

[6] V. Pascalutsa, V. Pauk, and M. Vanderhaeghen, Light-by-light scattering sum rules constraining meson transition form factors, Phys. Rev. D **85**, 116001 (2012).

[7] V. Pauk and M. Vanderhaeghen, Single meson contributions to the muon's anomalous magnetic moment, Eur. Phys. J. C **74**, 3008 (2014).

[8] A. A. Osipov, A. A. Pivovarov, and M. K. Volkov, The anomalous decay $f_1(1285) \to \rho\gamma$ and related processes, Phys. Rev. D **96**, 054012 (2017).

[9] A. I. Milstein and A. S. Rudenko, Consistent analysis of $f_1(1285)$ meson form factors, Phys. Lett. B **800**, 135117 (2020).

[10] A. Dorokhov, A. Martynenko, F. Martynenko, A. Radzhabov, and A. Zhevlakov, The LbL contribution to the muon g-2 from the axial-vector mesons exchanges within the nonlocal quark model, EPJ Web Conf. **212**, 05001 (2019).

[11] P. Roig and P. Sanchez-Puertas, Axial-vector exchange contribution to the hadronic light-by-light piece of the muon anomalous magnetic moment, Phys. Rev. D **101**, 074019 (2020).

[12] J. Leutgeb and A. Rebhan, Axial vector transition form factors in holographic QCD and their contribution to the anomalous magnetic moment of the muon, Phys. Rev. D **101**, 114015 (2020).

[13] L. Cappiello, O. Catà, G. D'Ambrosio, D. Greynat, and A. Iyer, Axial-vector and pseudoscalar mesons in the hadronic light-by-light contribution to the muon $(g-2)$, Phys. Rev. D **102**, 016009 (2020).

[14] M. Zanke, M. Hoferichter, and B. Kubis, On the transition form factors of the axial-vector resonance $f_1(1285)$ and its decay into e^+e^-, arXiv:2103.09829.

[15] A. Szczurek, Production of axial-vector mesons at e^+e^- collisions with double-tagging as a way to constrain the axial meson light-by-light contribution to the muon g-2 and the hyperfine splitting of muonic hydrogen, Phys. Rev. D **102**, 113015 (2020).

[16] R. Dickson *et al.* (CLAS Collaboration), Photoproduction of the $f_1(1285)$ meson, Phys. Rev. C **93**, 065202 (2016).

[17] N. I. Kochelev, M. Battaglieri, and R. De Vita, Exclusive photoproduction of $f_1(1285)$ meson off the proton in kinematics available at the Jefferson Laboratory experimental facilities, Phys. Rev. C **80**, 025201 (2009).

[18] S. K. Domokos, H. R. Grigoryan, and J. A. Harvey, Photoproduction through Chern-Simons term induced interactions in holographic QCD, Phys. Rev. D **80**, 115018 (2009).

[19] X.-Y. Wang and J. He, Analysis of recent CLAS data on $f_1(1285)$ photoproduction, Phys. Rev. D **95**, 094005 (2017).

[20] Y.-Y. Wang, L.-J. Liu, E. Wang, and D.-M. Li, Study on the reaction of $\gamma p \to f_1(1285)p$ in Regge-effective Lagrangian approach, Phys. Rev. D **95**, 096015 (2017).

[21] B.-G. Yu and K.-J. Kong, Photoproductions of $f_1(1285)$ and $\eta'(958)$ from the analysis of CLAS data with the Primakoff effect at high energies, Phys. Rev. D **102**, 054019 (2020).

[22] Y.-s. Oh, N. I. Kochelev, D.-P. Min, V. Vento, and A. V. Vinnikov, Anomalous f_1 exchange in vector meson photoproduction asymmetries, Phys. Rev. D **62**, 017504 (2000).

[23] D. Barberis *et al.* (WA102 Collaboration), A study of the centrally produced $\pi^+\pi^-\pi^+\pi^-$ channel in pp interactions at 450 GeV/c, Phys. Lett. B **413**, 217 (1997).

[24] D. Barberis *et al.* (WA102 Collaboration), A study of the $K\bar{K}\pi$ channel produced centrally in pp interactions at 450 GeV/c, Phys. Lett. B **413**, 225 (1997).

[25] D. Barberis *et al.* (WA102 Collaboration), A measurement of the branching fractions of the $f_1(1285)$ and $f_1(1420)$ produced in central pp interactions at 450 GeV/c, Phys. Lett. B **440**, 225 (1998).

[26] D. Barberis *et al.* (WA102 Collaboration), A spin analysis of the 4π channels produced in central pp interactions at 450 GeV/c, Phys. Lett. B **471**, 440 (2000).

[27] P. Lebiedowicz, J. Leutgeb, O. Nachtmann, A. Rebhan, and A. Szczurek, Central exclusive diffractive production of axial-vector $f_1(1285)$ and $f_1(1420)$ mesons in proton-proton collisions, Phys. Rev. D **102**, 114003 (2020).

[28] C. Ewerz, M. Maniatis, and O. Nachtmann, A model for soft high-energy scattering: Tensor Pomeron and Vector Odderon, Ann. Phys. (Amsterdam) **342**, 31 (2014).

[29] M. Lutz *et al.* (PANDA Collaboration), Physics performance report for PANDA: Strong interaction studies with antiprotons, arXiv:0903.3905.

[30] A. Szczurek and P. Lebiedowicz, Exclusive scalar $f_0(1500)$ meson production for energy ranges available at the GSI Facility for Antiproton and Ion Research (GSI-FAIR) and at the Japan Proton Accelerator Research Complex (J-PARC), Nucl. Phys. **A826**, 101 (2009).

[31] P. Lebiedowicz, O. Nachtmann, and A. Szczurek, Exclusive central diffractive production of scalar and pseudoscalar mesons; tensorial vs vectorial Pomeron, Ann. Phys. (Amsterdam) **344**, 301 (2014).

[32] R. Machleidt, K. Holinde, and C. Elster, The bonn meson-exchange model for the nucleon–nucleon interaction, Phys. Rep. **149**, 1 (1987).

[33] M. Kirchbach and D. O. Riska, The coupling of the $f_1(1285)$ meson to the isoscalar axial current of the nucleon, Nucl. Phys. **A594**, 419 (1995).

[34] E. L. Bratkovskaya, V. Y. Grishina, L. A. Kondratyuk, M. Büscher, and W. Cassing, Production of a_0 mesons in pp and pn reactions, J. Phys. G **28**, 2423 (2002).

[35] L. A. Kondratyuk, E. L. Bratkovskaya, V. Y. Grishina, M. Büscher, W. Cassing, and H. Stroher, Near-threshold production of $a_0(980)$ mesons in πN and NN collisions and a_0-f_0 mixing, Phys. At. Nucl. **66**, 152 (2003).

[36] P. Lebiedowicz, O. Nachtmann, and A. Szczurek (to be published).

[37] K. Nakayama, A. Szczurek, C. Hanhart, J. Haidenbauer, and J. Speth, Production of ω mesons in proton-proton collisions, Phys. Rev. C **57**, 1580 (1998).

[38] G. Höhler and E. Pietarinen, The ρNN vertex in vector-dominance models, Nucl. Phys. **B95**, 210 (1975).

[39] K. Nakayama, J. W. Durso, J. Haidenbauer, C. Hanhart, and J. Speth, ϕ-Meson production in proton-proton collisions, Phys. Rev. C **60**, 055209 (1999).

[40] P. Mergell, U.-G. Meissner, and D. Drechsel, Dispersion-theoretical analysis of the nucleon electromagnetic form factors, Nucl. Phys. **A596**, 367 (1996).

[41] G. Janssen, K. Holinde, and J. Speth, $\pi\rho$ correlations in the NN potential, Phys. Rev. C **54**, 2218 (1996).

[42] T. Sato and T.-S. H. Lee, Meson-exchange model for πN scattering and $\gamma N \to \pi N$ reaction, Phys. Rev. C **54**, 2660 (1996).

[43] K. Tsushima and K. Nakayama, Near-threshold ω and ϕ meson productions in pp collisions, Phys. Rev. C **68**, 034612 (2003).

[44] K. Nakayama, Y. Oh, J. Haidenbauer, and T.-S. H. Lee, On the sign of the $\pi - \rho - \omega$ coupling constant, Phys. Lett. B **648**, 351 (2007).

[45] P. Lebiedowicz, O. Nachtmann, and A. Szczurek, Central exclusive diffractive production of $K^+K^-K^+K^-$ via the intermediate $\phi\phi$ state in proton-proton collisions, Phys. Rev. D **99**, 094034 (2019).

[46] A. Donnachie, H. G. Dosch, P. V. Landshoff, and O. Nachtmann, Pomeron physics and QCD, Cambridge Monogr. Part. Phys., Nucl. Phys., Cosmol. **19**, 1 (2002).

[47] P. Zyla *et al.* (Particle Data Group), Review of particle physics, Prog. Theor. Exp. Phys. **2020**, 083C01 (2020).

[48] Y. Oh and T.-S. H. Lee, ρ meson photoproduction at low-energies, Phys. Rev. C **69**, 025201 (2004).

[49] P. Lebiedowicz, O. Nachtmann, and A. Szczurek, Exclusive diffractive production of $\pi^+\pi^-\pi^+\pi^-$ via the intermediate $\sigma\sigma$ and $\rho\rho$ states in proton-proton collisions within tensor Pomeron approach, Phys. Rev. D **94**, 034017 (2016).

[50] K. Nakayama, J. Haidenbauer, and J. Speth, The reactions $pn \to d\omega$ and $pn \to d\phi$ near threshold, Phys. Rev. C **63**, 015201 (2000).

[51] L. P. Kaptari and B. Kämpfer, Combined analysis of near-threshold production of ω and ϕ mesons in nucleon-nucleon collisions within an effective meson-nucleon model, Eur. Phys. J. A **23**, 291 (2005).

[52] P. Lebiedowicz, O. Nachtmann, and A. Szczurek, Central production of ρ^0 in pp collisions with single proton diffractive dissociation at the LHC, Phys. Rev. D **95**, 034036 (2017).

[53] G. Alexander, O. Benary, G. Czapek, B. Haber, N. Kidron, B. Reuter, A. Shapira, E. Simopoulou, and G. Yekutieli, Proton-proton interactions at 5.5 GeV/c, Phys. Rev. **154**, 1284 (1967).

[54] G. Agakishiev *et al.* (HADES Collaboration), The high-acceptance dielectron spectrometer HADES, Eur. Phys. J. A **41**, 243 (2009).

[55] J. Adamczewski-Musch *et al.* (HADES and PANDA@-HADES Collaborations), Production and electromagnetic decay of hyperons: A feasibility study with HADES as a phase-0 experiment at FAIR, Eur. Phys. J. A **57**, 138 (2021).

[56] G. Barucca *et al.* (PANDA Collaboration), PANDA phase one, Eur. Phys. J. A **57**, 184 (2021).

[57] I. Fröhlich *et al.*, Pluto: A Monte Carlo simulation tool for hadronic physics, *Proc. Sci.*, ACAT2007 (2007) 076 [arXiv:0708.2382].

[58] I. Fröhlich, T. Galatyuk, R. Holzmann, J. Markert, B. Ramstein, P. Salabura, and J. Stroth, Design of the Pluto Event Generator, J. Phys. Conf. Ser. **219**, 032039 (2010).

[59] I. Fröhlich *et al.*, A versatile method for simulating $pp \to ppe^+e^-$ and $dp \to pne^+e^-p_{\mathrm{spec}}$ reactions, Eur. Phys. J. A **45**, 401 (2010).

[60] Z. Ouyang, J.-J. Xie, B.-S. Zou, and H.-S. Xu, Theoretical study on $pp \to pn\pi^+$ reaction at medium energies, Int. J. Mod. Phys. E **18**, 281 (2009).

[61] X. Cao, J.-J. Xie, B.-S. Zou, and H.-S. Xu, Evidence of $N^*(1535)$ resonance contribution in the $pn \to d\phi$ reaction, Phys. Rev. C **80**, 025203 (2009).

[62] X. Cao, B.-S. Zou, and H.-S. Xu, Phenomenological analysis of the double-pion production in nucleon-nucleon collisions up to 2.2 GeV, Phys. Rev. C **81**, 065201 (2010).

[63] X. Cao, B.-S. Zou, and H.-S. Xu, Phenomenological study on the $\bar{p}N \to \bar{N}N\pi\pi$ reactions, Nucl. Phys. **A861**, 23 (2011).

[64] X. Cao and X.-G. Lee, The role of the $N^*(1535)$ in η' production, Phys. Rev. C **78**, 035207 (2008).

[65] F. Huang, H. Haberzettl, and K. Nakayama, Combined analysis of η' production reactions: $\gamma N \to \eta' N$, $NN \to NN\eta'$, and $\pi N \to \eta' N$, Phys. Rev. C **87**, 054004 (2013).

[66] A. Sibirtsev, C. Elster, S. Krewald, and J. Speth, Photoproduction of η'-mesons from the proton, AIP Conf. Proc. **717**, 837 (2004).

[67] H. P. Morsch *et al.*, Radial Excitation of the Nucleon to the $P_{11}(1440\ \mathrm{MeV})$ Resonance in Alpha-Proton Scattering, Phys. Rev. Lett. **69**, 1336 (1992).

[68] L. Alvarez Ruso, E. Oset, and E. Hernandez, Theoretical study of the $NN \to NN\pi\pi$ reaction, Nucl. Phys. **A633**, 519 (1998).

[69] E. Hernandez and E. Oset, Isoscalar Roper excitation in the $pp \to pp\pi^0$ reaction close to threshold, Phys. Rev. C **60**, 025204 (1999).

[70] S. Danieli, A. Shapira, Y. Eisenberg, B. Haber, E. E. Ronat, G. Yekutieli, and J. Grunhaus, Four- and five-pion production in pp collisions at 6.92 GeV/c, Nucl. Phys. **B27**, 157 (1971).

[71] F. Aceti, J. Dias, and E. Oset, $f_1(1285)$ decays into $a_0(980)\pi^0$, $f_0(980)\pi^0$ and isospin breaking, Eur. Phys. J. A **51**, 48 (2015).

[72] N. N. Achasov and G. N. Shestakov, Proposal to look for the anomalous isotopic symmetry breaking in central diffractive production of the $f_1(1285)$ and $a_0^0(980)$ resonances at the LHC, Phys. Rev. D **97** (2018) 054033.

[73] N. N. Achasov and G. N. Shestakov, Strong isospin symmetry breaking in light scalar meson production, Phys. Usp. **62**, 3 (2019).

[74] F. Aceti, J.-J. Xie, and E. Oset, The $K\bar{K}\pi$ decay of the $f_1(1285)$ and its nature as a $K^*\bar{K} - cc$ molecule, Phys. Lett. B **750**, 609 (2015).

[75] J.-J. Xie, G. Li, and X.-H. Liu, Radiative decays of $f_1(1285)$ as the $K^*\bar{K}$ molecular state, Chin. Phys. C **44**, 114104 (2020).

[76] R. A. Kycia, P. Lebiedowicz, and A. Szczurek, Decay: A Monte Carlo library for the decay of a particle with ROOT compatibility, Commun. Comput. Phys. **30**, 942 (2021).

[77] D. V. Amelin *et al.*, Study of the decay $f_1(1285) \to \rho^0(770)\gamma$, Z. Phys. C **66**, 71 (1995).

[78] S. Ishida, K. Yamada, and M. Oda, Radiative decays of light-quark S- and P-wave mesons in the covariant oscillator quark model, Phys. Rev. D **40**, 1497 (1989).